이학박사 학위논문

Characteristic electrochemical features of nanoparticles and microemulsions

나노입자와 마이크로에멀션의 전기화학적 특징에 관한 연구

2017 년 8 월

서울대학교 대학원
화학부 전기분석화학전공
한 동 협

A Dissertation entitled

Characteristic electrochemical features of nanoparticles and microemulsions

By Dong Hyeop Han
Major: Electrochemistry

Submitted as partial fulfillment of the requirements for the Doctor of Philosophy degree in Chemistry

Advisor: Prof. Taek Dong Chung

Seoul National University
August, 2017

Abstract

Research on energy to replace fossil fuels has been one of the most important topics for decades to address the problems of depleting fossil fuels and increasing environmental pollution. Despite numerous efforts, the energy consumption is steadily increasing globally and most of the energy needs are still being met by fossil fuels. Therefore, research on new energy conversion technologies and storage devices has become very important.

One of the important requisites for fabricating in energy conversion devices is choosing an appropriate catalytic material for the electrochemical reaction. Recently, much research has been conducted on the synthesis and application of nanoparticles for improving the efficiency of such catalyst materials. The physical and chemical properties of nanoparticles are different from those of bulk materials. They have a very large surface area compared to their volume, and their electrochemical activity is superior to bulk materials because of their dominant surface properties.

However, the electrochemical properties of nanoparticles and their causes are still not fully understood.

Energy storage devices are also attracting attention from another perspective. In general, energy is consumed in the form of electricity, however, the supply and consumption of electrical energy are not always balanced. In order to effectively solve these problems, an electric energy storage system needs to be developed that stores the remaining electricity and draw it out when required. Among the various energy storage technologies, redox flow battery is attracting attention because of its ability to easily control the power and capacity. Typical Redox flow batteries include Br−polysulfide and Zn−Br, which involve the redox reactions of Br^-/Br_2. However, problem with these systems is that the electrochemically generated Br_2 passes through the separator and causes self−discharge. To prevent this, quaternary ammonium bromides that capture Br_2 and form microemulsions are usually added to the systems. Recently, it has been reported that this microemulsions participate not only in capturing Br_2 but also in electrochemical reactions,

however the mechanism is not clear.

As mentioned above, small particles such as nanoparticles and microemulsions participate in electrochemical reactions in energy conversion and storage devices. However, many studies focused on material aspects and did not fully explain the role of such small particles and their electrochemical properties in electrochemical reactions. This dissertation describes two case studies to investigate the effect of the fundamental electrochemical characteristics of such small particles on energy conversion and storage devices.

First, the oxidation stability of gold nanoparticles in an electrochemical environment was investigated. Using a diblock copolymer, we synthesized different arrays of nanoparticles, which can uniformly control the size and interparticle spacing to the nanometer scale on the substrate electrode. Then, we observed the change in the oxidation reactivity according to the size and spacing of the nanoparticles. The surface coverage, total amount of gold deposited on the substrate, also changed when the size and spacing parameters were adjusted. Experimental and

theoretical results showed that the surface coverage is more influential than diameter on the oxidation reaction under experimental conditions.

Secondly, It is studied how the bromine complexing agent electrochemically forms emulsions and how the emulsions participate in the Br^-/Br_2 half reaction with respect to redox flow batteries. The electrochemical properties of microemuslion was investigated by acquiring chronoamperometric signals and confocal spectroscopic images simultaneously. The experimental results show that microemulsions heterogeneously generate on the electrode surface and the adsorbed emulsions increase the oxidation current. Furthermore, a current spike in the chronoamperogram was generated by a collision of emulsion. It is proved that the formation and collision of the emulsion had a great influence on the Br^- oxidation.

These results show a new understanding of the underlying mechanisms through which small particles that affect energy conversion and storage devices, and are expected to provide new directions to the research and development of energy

conversion technologies and storage devices.

Keywords: energy conversion and storage devices, catalyst, nanoparticle, microemulsion, confocal microscopy, electrochemical properties

Student number: 2011-20312

Contents

List of Figures

(51 k-18 k) micelles

[Fig. 2-4] TEM image of Au NP arrays fabricated from PS-P4VP (51 k-18 k)

[Fig. 2-5] LSVs from arrays of Au NPs on ITO/glass substrate in 10 mM KBr and 0.1 M $HClO_4$ at 5 mVs^{-1}. The currents were normalized by setting the LSVs to have the same oxidation peak current (I_p) for clearer identification of shifts in oxidation peak potential (E_p).

[Fig. 2-6] Theoretical E_p as a function of diameter of NPs based on the Plieth equation. Solid line is on the basis of theoretical values assuming that z is 3 and E_p (bulk) is 1.067 V that was measured at an Au wafer. The experimental results (▲) indicate that the Plieth curve shifted to the dashed line (---)

[Fig. 2-7] Linear relationship between E_p (■) and ln (Q)

[Fig. 3-15] The images tracing droplets that approach the electrode surface as a function of time. The targeted droplets (indicated by yellow and red circles) as time elapses at 0.925 V applied. They drift in random direction that is switched by collision with another droplet.

[Fig. 3-16] Images at the moment the emulsion collides with surface of a Pt wire electrode. White arrows indicate the position of the targeted droplet. The time elapsed at 1.0 V (a) 16.96 s, (b) 16.99 s, (c) 17.02 s, (d) 17.62 s, (e) 18.04 s, (f) 18.34 s, respectively. Scale bar = 2 μm

[Fig. 3-17] Images at the moment the emulsion collides with the surface of a Pt wire electrode. White arrows indicate the position of the targeted droplet. 1.0 V was applied to the electrode. The entire images, out of which 6 images were selected, were collected at intervals of 0.15 s. The time from the first image is (a) 0 s, (b) 0.15 s, (c) 0.45 s, (d) 1.35 s, (e) 1.95 s, (f) 3.60 s, respectively. Scale bar = 2 μm.

[Fig. 3-18] Images at the moment the emulsion collides with the surface of a Pt wire electrode. White arrows indicate the position of the targeted droplet. A 1.0 V was applied to the electrode. The entire images, out of which 6 images were selected, were collected at intervals of 0.15 s. The time from the first image is (a) 0 s, (b) 0.15 s, (c) 1.35 s, (d) 2.10 s, (e) 2.40 s, (f) 3.00 s, respectively. Scale bar = 2 μm.

[Fig. 3-19] Images at the moment the emulsion collides with the surface of a Pt wire electrode. White arrows indicate the position of the targeted droplet. A 1.0 V was applied to the electrode. The entire images, out of which 6 images were selected, were collected at intervals of 0.15 s. The time from the first image is (a) 0 s, (b) 0.15 s, (c) 0.30 s, (d) 0.60 s, (e) 1.35 s, (f) 2.25 s, respectively. Scale bar = 2 μm.

[Fig. 3-20] Images at the moment the emulsion collides

with the surface of a Pt wire electrode. White arrows indicate the position of the targeted droplet. A 1.0 V was applied to the electrode. The entire images, out of which 6 images were selected, were collected at intervals of 0.15 s. The time from the first image is (a) 0 s, (b) 0.15 s, (c) 0.30 s, (d) 2.70 s, (e) 3.45 s, (f) 4.05 s, respectively. Scale bar = 2 μm.

[Fig. 3-21] Chronoamperogram from a Pt UME monitored by confocal microscopy. (black line) Red dots are the moments droplets collide with the electrode surface.

[Fig. 3-22] Chronoamperogram from a Pt UME monitored by confocal microscopy. (black line) Red dots are the moments droplets collide with the electrode surface. Succeeding spike current is marked by series of number.

[Fig. 3-23] Sequence of images at the number shown in Fig. 3-22. A droplet collides with surface of a Pt UME.

White arrows indicate the position of the targeted droplet. A 1.0 V was applied to the electrode, and each sequence of images were collected at intervals of 0.0195 s, Scale bar = 2 μm

[Fig. 3-24] The confocal microscopy images of the spike at 22.24 s, which is the largest spike in Fig. 3-21. Images of just before the emulsion collision (a) 22.20 s, (b) 22.22s. An image at collision moment (c) 22.24s. The image for the next spike in the i-t curve (d) 22.76 s.

[Fig. 3-25] Images of the moment a droplet collides with the surface of a Pt UME. White arrows indicate the position of the droplet traced. The time elapsed at 1.0 V is (a) 20.19 s, (b) 20.21 s, (c) 20.23 s, (d) 20.31 s, (e) 20.36 s, (f) 20.42 s, respectively. Scale bar = 2 μm

[Fig. 3-26] Images at the moment the emulsion collides with the surface of a Pt UME. White arrows indicate the position of the targeted droplet. A 1.0 V was applied to the

electrode. The entire images, out of which 6 images were selected, were collected at intervals of 0.15 s. The time from the first image is (a) 0 s, (b) 1.48 s, (c) 2.74 s, (d) 3.48 s, (e) 3.58 s, (f) 3.69 s, respectively. Scale bar = 2 μ m.

[Fig. 3-27] Images at the moment the emulsion collides with the surface of a Pt UME. White arrows indicate the position of the targeted droplet. A 1.0 V was applied to the electrode. The entire images, out of which 6 images were selected, were collected at intervals of 0.15 s. The time from the first image is (a) 0 s, (b) 0.3 s, (c) 0.45 s, (d) 1.2 s, (e) 1.95 s, (f) 2.85 s, respectively. Scale bar = 2 μ m.

[Fig. 3-28] Images at the moment the emulsion collides with the surface of a Pt UME. White arrows indicate the position of the targeted droplet. A 1.0 V was applied to the electrode. The entire images, out of which 6 images were

selected, were collected at intervals of 0.15 s. The time from the first image is (a) 0 s, (b) 0.60 s, (c) 1.35 s, (d) 1.65 s, (e) 2.84 s, (f) 2.99 s, respectively. Scale bar = 2 μ m.

[Fig. 3-29] Chronoamperogram and confocal microscopy images at the moment the droplets grow on the surface of a Pt wire electrode. The time elapsed at 0.85 V (a) 0 s, (b) 5 s, (c) 15 s, (d) 30 s, respectively. Scale bar = 5 μm. (e) Chronoamperogram at 0.85 V

List of Tables

1. Introduction

1.1 Background and Overview

In recent times, energy has become one of the most important research topics, because of the rapid depletion of fossil fuels and the increasing environmental problems owing to the use of fossil fuels. Hence, many efforts have been made in the past to develop energy technologies that can replace fossil fuels. However, 86% of the world' s energy consumption is still met through fossil fuels and only less than 3% is obtained by using renewable energy technologies. (**Fig. 1-1**) In addition, much of the energy is being consumed in the form of electrical energy, and the demand for electricity is expected to double globally by 2050.[1] Therefore, research on new energy conversion technologies and storage devices to solve these problems has become very important.

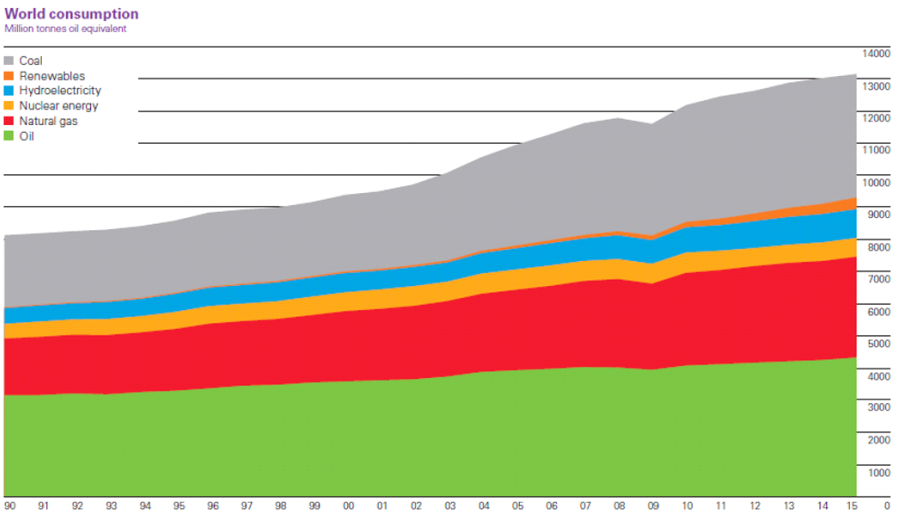

Fig. 1-1 Graph of world primary energy consumption changes over the year.[2]

First, the key part of the energy conversion devices is the interface between the electrode and the electrochemical species where energy conversion takes place. The catalyst promotes electrochemical reactions at the interface and is the most important part of energy conversion devices such as fuel cells, solar cells and redox flow batteries. Over the decades, numerous efforts have been made to develop new catalytic materials, but they failed to completely solve the

energy problems. A possible reason for this situation is that we still do not understand the origin of the catalytic phenomenon. For example, an oxygen reduction reaction is an important reaction that takes place on the typical cathode of a fuel cell. However, the mechanism of the relatively simple oxygen reduction reaction is still not fully understood, and despite the numerous efforts to replace platinum, which is a costly catalyst, platinum-based catalysts are still used because they show the highest catalytic properties of oxygen reduction.[3] One strategy for improving the performance of non-platinum catalysts in oxygen reduction reaction or various catalyst materials in other reactions is to make their nanoparticles.

Nanoparticles have been a subject of great interest in the last few years because they have very distinct mechanical, electrical, optical and chemical properties from those of bulk materials.[4] Nanoparticles have been applied to the fields of sensing, separation, plasmonics, nanoelectronics, and electrochemical catalysts because of their favorable properties.[5, 6] The nanoparticle electrode has advantages

such as large surface area, high mass transfer rate, good catalytic property, and efficient control over the local environment in an electrochemical system as compared with those achieved with bulk electrodes.[7, 8]

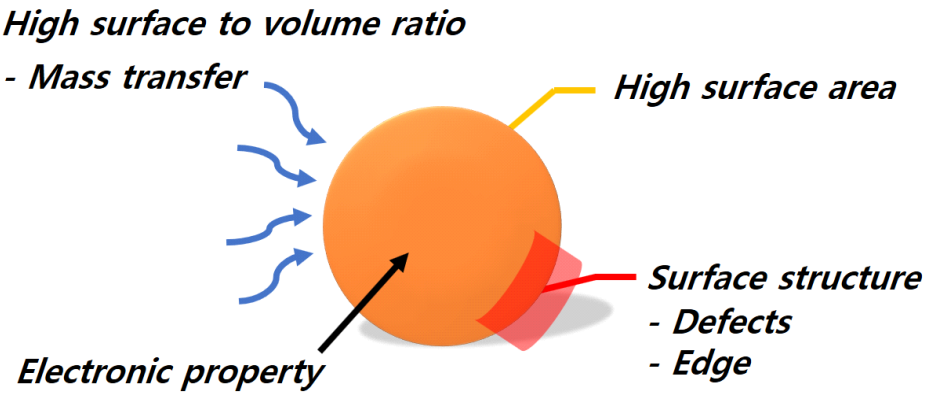

Fig. 1-2 Unique properties of nanoparticle

Gold nanoparticles (Au NPs) are used as the representative nanoparticles in electrochemical environments. Au NPs are particularly well suited for electrochemical analysis because of their good biological compatibility and excellent conducting capabilities.[9] These advantages of Au NPs are widely used as genosensors and immunosensors

with high sensitivity. Bulk gold does not catalyze the oxidation and reduction of hydrogen peroxide. However, Au NPs have a large surface area relative to the volume and exhibit good catalytic effects because of their interface-dominated properties.[10] Also, It has been reported that Au NPs show good catalytic activity for important electrochemical reactions in fuel cells such as the reduction of dioxygen and oxidation of methanol.[11-14] Therefore, investigation of the unique properties of these Au NPs in electrochemical environments is important, as it will help reveal the origin of the catalytic effect of the nanoparticles.

New eco-friendly energy production methods have also been researched and developed in an effort to replace existing fossil fuel-based power plants. Typical renewable energy sources include solar energy and wind power. Power plants using these energy sources have recently been built and they are being expanded globally.[15] However, such a "green" energy source has a disadvantage in that the electricity production varies, depending on the weather, and

the electric grid used currently is not designed to work with such a disadvantage.[16] Also, the energy consumption is not constant over time. Consumers use more energy in the daytime, and the consumption increases significantly during summers. Extreme events such as power outages occur when power generation fails to catch up. For these reasons, there is a growing need for electrical energy storage (EES) to bridge the gap between energy production and consumption.[2, 17] Among the various energy storage technologies for EES, redox flow battery (RFB) is attracting attention as an ideal technology considering the system size for utilizing solar energy (1 kW ~ 550 MW) and 2.5 ~ 7.5 MW of general power using wind turbine.[18]

RFB is a type of battery that stores energy in the reduced and oxidized species.[19] Schematic representation of RFB is provided in **Fig. 1-3**. Two redox species are stored in external tanks in the form of dissolved species in the each electrolyte. Electrolytes are first pumped to the electrodes, following which electrochemical reactions occur at the electrode that convert the chemical energy into electrical

energy (discharge) or vice versa (charge).[17]

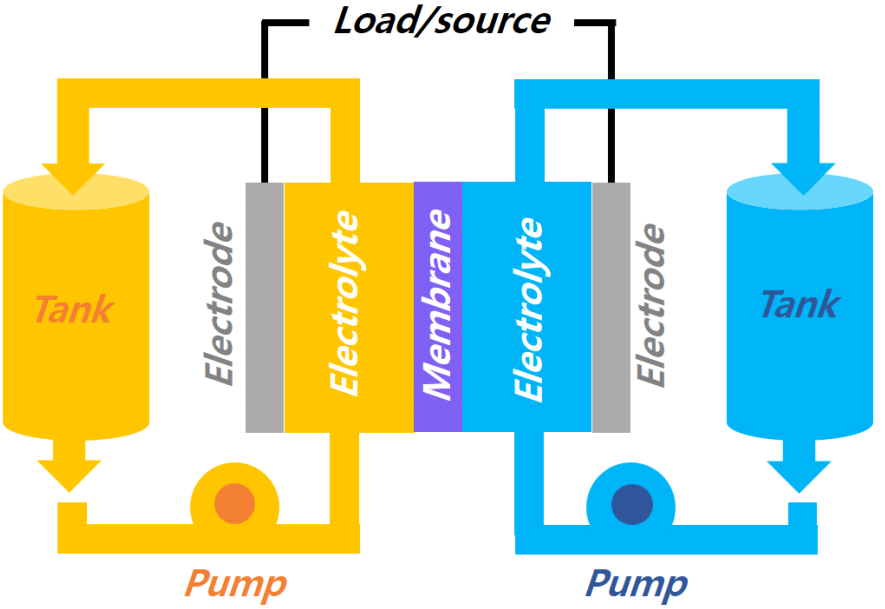

Fig. 1-3 Schematic representation of redox flow battery

RFB has many advantages (ex. Cost, flexible operations), one of the most important advantages is that the power and energy storage capacity of the RFB can be easily controlled. The power can be controlled by varing the size of the electrode and the number of unit cells of the battery, and the capacity can be controlled by changing the concentration and total amount of the redox species contained in the electrolyte.[17] This is what makes RFB suitable as an EES for future green energy grid.

Representative RFB systems include Br−polysulfide and Zn−Br, which use a Br^-/Br_2 redox reaction as a half−cell electrochemical reaction.[2, 17, 19] However, the use of reaction as a half−cell reaction is a problem, electrochemically generated Br_2 cause self−discharging through the membrane, thereby lowering the efficiency of the cell. To prevent this problem, quaternary ammonium bromides (QBr' s), which can capture Br_2, are added to the aqueous electrolyte to form an organic microemulsion of QBr_{2n+1}.

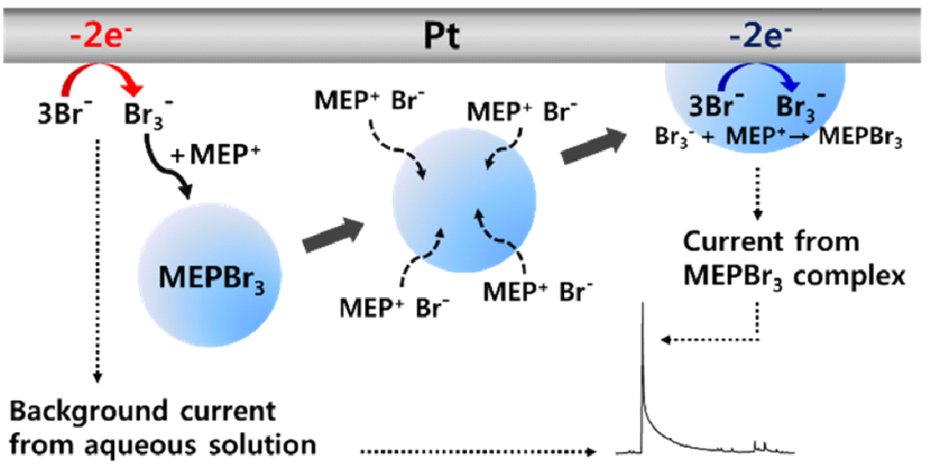

Fig. 1−4 Schematic representation of a presented Br^- reaction pathway related with $MEPBr_3$ emulsion [20]

It is recently revealed that this microemulsion not only plays a role in capturing Br_2 but also participates in the Br^-/Br_2 reaction.(**Fig. 1-4**) However, the electrochemistry of the microemulsion has not yet been clarified.

As stated above, numerous researchers are making many attempts to solve the energy problem. However, a complete solution has still not been achieved. This is because the underlying mechanism of important electrochemical reactions in energy conversion and storage devices has not been revealed yet. In particular, small particles such as nanoparticles and microemulsions are widely used for promoting electrochemical reactions or suppressing side reactions. However, physicochemical properties of these particles are different from bulk materials, moreover, the characteristics in electrochemical environments have not been completely understood yet. Therefore, it is important to study the electrochemical properties of such small particles. This thesis is divided into two main chapters. In Chapter 2, electrooxidative dissolution of uniformly distributed Au NPs is reported.[21] To study the inherent electrochemical

properties of Au NPs, different arrays of Au NPs were synthesized without using any extra adhesion layer or capping agent. Diblock copolymer micelles were used to fabricate the arrays of Au NPs, where not only the diameter of the particles but also interparticle spacing were finely controlled. The surface coverage, total amount of gold synthesized on the substrate, also changed when the size and spacing of Au NPs were varied. The peak potential for electrochemical oxidation shifted greater as a function of coverage of NPs than the size. Chapter 3 discusses *in situ* confocal microscopy study of electrochemical generation and collision of microemulsions in a bromide redox system. It is reported how the bromine complexing agent forms emulsions and how the emulsions participate in the Br^-/Br_2 half reaction with respect to redox flow batteries. Through electrochemical signals and confocal spectroscopic images acquired simultaneously, it was revealed that microemulsions heterogeneously generate on the electrode surface and increase of current. Furthermore, current spikes in a chronoamperogram originate from collisions of emulsions. A

comparison study provided compelling evidence supporting that electrochemistry at the interface between the electrode and the droplet makes a significant contribution to the overall Br^- oxidation reaction. Finally, Chapter 4 summarizes the conclusion and contributions of this study.

1.2 References

[1] Dunn, B., Kamath, H., Tarascon, J.-M., *Science,* 2011, *334*, 928.

[2] *BP Statistical Review of World Energy*, 2016.

[3] Gasteiger, H. A., Marković, N. M., *Science,* 2009, *324*, 48.

[4] Arico, A. S., Bruce, P., Scrosati, B., Tarascon, J.-M., van Schalkwijk, W., *Nat. Mater.,* 2005, *4*, 366.

[5] Ivanova, O. S., Zamborini, F. P., *Anal. Chem.,* 2010, *82*, 5844.

[6] Masitas, R. A., Zamborini, F. P., *J. Am. Chem. Soc.,* 2012, *134*, 5014.

[7] Katz, E., Willner, I., Wang, J., *Electroanalysis,* 2004, *16*, 19.

[8] Welch, C. M., Compton, R. G., *Anal. Bioanal. Chem.,* 2006, *384*, 601.

[9] Guo, S., Wang, E., *Anal. Chim. Acta,* 2007, *598*, 181.

[10] Yu, A., Liang, Z., Cho, J., Caruso, F., *Nano Lett.,* 2003, *3*, 1203.

[11] Hernández, J., Solla-Gullón, J., Herrero, E., Aldaz, A.,

Feliu, J. M., *Electrochim. Acta,* 2006, *52*, 1662.

[12] Crespilho, F. N., Nart, F. C., Oliveira Jr, O. N., Brett, C. M. A., *Electrochim. Acta,* 2007, *52*, 4649.

[13] Cheng, W., Dong, S., Wang, E., *J. Phys. Chem. B,* 2004, *108*, 19146.

[14] El-Deab, M. S., Ohsaka, T., *J. Electroanal. Chem.,* 2003, *553*, 107.

[15] Abdmouleh, Z., Alammari, R. A. M., Gastli, A., *Renew. Sust. Energ. Rev.,* 2015, *45*, 249.

[16] Cappers, P., MacDonald, J., Goldman, C., Ma, O., *Energ. Policy,* 2013, *62*, 1031.

[17] Yang, Z., Zhang, J., Kintner-Meyer, M. C. W., Lu, X., Choi, D., Lemmon, J. P., Liu, J., *Chem. Rev.,* 2011, *111*, 3577.

[18] Winsberg, J., Hagemann, T., Janoschka, T., Hager, M. D., Schubert, U. S., *Angew. Chem. Int. Ed.,* 2017, *56*, 686.

[19] Ponce de León, C., Frías-Ferrer, A., González-García, J., Szánto, D. A., Walsh, F. C., *J. Power Sources,* 2006, *160*, 716.

[20] Park, S., Kim, H., Chae, J., Chang, J., *J. Phys. Chem. C,*

2016, *120*, 3922.

[21] Han, D., Kim, S.-S., Kim, Y.-R., Sohn, B.-H., Chung, T. D., *Electrochem. Commun.,* 2015, *53*, 11.

2. Surface Coverage and Size Effect on Electrochemical Oxidation of Uniform Gold Nanoparticles

2.1 Introduction

Electrodes with nanostructured surfaces have been investigated for a variety of applications such as electrochemical catalysis, sensing, separations, plasmonics and nanoelectronics.[1, 2] It is because the physical and chemical properties of 'nano electrodes' are distinct from those of flat electrodes composed of the same materials. While a great deal of efforts have been made to unravel the origin of the difference in due course, it is still far to reach complete understanding.[3] In particular, NPs on an electrode substrate tend to be dissolved as a consequence of electrochemical oxidation but the underlying mechanism responsible for that behaviour is unclear yet.

Plieth theoretically predicted negative shift of redox potential with decreasing radius of NPs owing to surface free energy[4], which was followed by subsequent theoretical reports of similar results.[5, 6] These inspired many researchers to experimentally tackle this issue by conventional electrochemical techniques such as voltammetry. It was ascertained that the electrochemical oxidation of Au[1, 2], Ag[3, 7], Pt[8, 9], Pd[10] and Cu[11] NPs is significantly influenced by the radius of those. Compton and co-workers approached in another point of view, *i.e.* diffusion of metal ions dissolved from metal NPs.[12-14] Recently, they derived the analytical expression of anodic stripping voltammetry of metal NPs under the consideration of mass transport as well as thermodynamic conditions, and the mass transport effects experimentally investigated by the effect of surface coverage of NPs.[3] However, they could not experimentally corroborate their hypothesis due to clustering of Ag NPs.

To address this issue, it is an effective strategy to prepare arrays of NPs where size and spacing of those are controlled precisely. But it remains a challenging task due to the lack of appropriate technology and/or method to make it possible. In this work, we fabricated Au NPs arrays without an adlayer on ITO/glass electrode using diblock copolymer micelles. From a monolayer of diblock copolymer micelles, we obtained well aligned Au NPs that are free from agglomeration throughout the experiment.[15, 16] The diameter of the Au NPs and inter-particle spacing among them were sophisticatedly tuned in the range of 4 ~ 9 nm and 30 ~ 60 nm, respectively. With this novel array, we were able to examine voltammetric behaviour that varied with diameter and coverage of pure Au NPs.

2.2 Experimental

2.2.1. Fabrication of array of Au nanoparticles

Four polystyrene-*block*-poly(4-vinyl pyridine) (PS-P4VP) diblock copolymers (M_n : 25 k-7 k, PDI = 1.10; M_n : 32 k-13 k, PDI = 1.08; M_n : 48k-21k, PDI = 1.14; M_n : 51 k-18 k, PDI = 1.15) were purchased from Polymer Source Inc. PS-P4VP copolymers were dissolved in toluene, a strongly selective solvent for PS blocks, to yield a 0.5 wt% spherical micellar solution, which was stirred for 24 h at room temperature and for 3 h at 85 °C and then cooled to room temperature. $HAuCl_4$, a precursor of Au nanoparticles, was added to the micellar solution. The molar ratio of precursors to pyridine units in the P4VP block was 0.5 for all PS-P4VP micelles. Prior to spin-coating, Indium tin oxide (ITO)-coated glass (15~20 Ω/sq) were cleaned by ultrasonication in isopropanol, acetone, and methanol, and were dried with nitrogen. Then a single-layered film of PS-P4VP micelles containing precursors of Au nanoparticles

was spin-coated onto an ITO substrate for 60 s at 4000 rpm for PS-P4VP (25 k-7 k), PS-P4VP (32 k-13 k) and PS-P4VP (51 k-18 k), and at 2000 rpm for PS-P4VP (51 k-18 k) and PS-P4VP (48 k-21 k). To synthesize the nanoparticles along with the removal of the copolymer, substrates were treated with oxygen plasma etching for 5 min (100 W, 38 mTorr).

2.2.2. Electrochemical measurements

Linear sweep voltammograms were obtained with a CHI 604B electrochemical workstation (CH instruments). The electrochemical cell consisted of three electrodes. For working electrode, Au nanoparticles decorated ITO-coated glass electrode or no-decorated one were used. The geometric surface area was 0.28 cm^2. A platinum wire was used as a counter electrode and Ag/AgCl as a reference electrode. 0.1 M perchloric acid containing 0.01 M potassium bromide was used for electrochemical oxidation experiments.

All plots were obtained after bubbling the solution with N_2 for 15 min. The results have been acquired at least three repetitive measurements under respective conditions.

2.3 Results and Discussion

PS-P4VP diblock copolymers micelles containing $HAuCl_4$ in core region were spin-coated onto ITO/glass substrates at various rotational speed (v) to form a monolayered micellar film (**Fig. 2-1**), which can act as a nanotemplate to yield arrays of NPs (**Fig. 2-2**). TEM image in **Fig. 2-3** shows a single-layered film of PS-P4VP micelles spin-coated on the substrate after selective I_2 staining of P4VP core blocks. From this micellar film, we synthesized arrays of Au NPs along with the removal of copolymers by the treatment of oxygen plasma as shown in **Fig. 2-4**. We confirmed that hexagonally-ordered Au NPs were successfully prepared without aggregation among individual NPs. Moreover, we were able to precisely control the diameter and spacing in nanoscale by molecular weights of copolymers as well as rotational speed for spin-coating. (**See Table 2-1**)

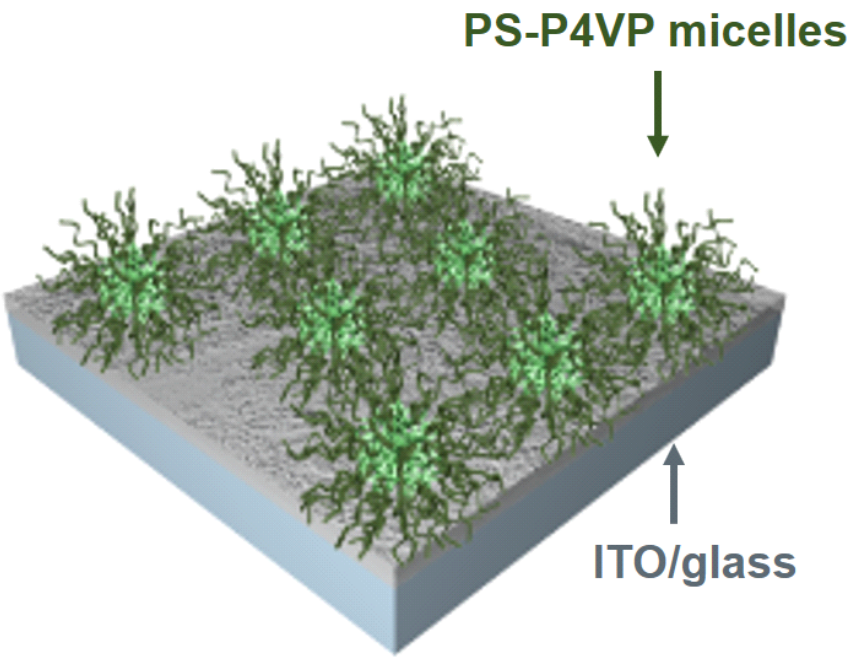

Fig. 2-1 Schematic diagram for fabrication of an array of Au NPs. A single-layered film of PS-P4VP micelles is enclosed $HAuCl_4$ in core region on the ITO/glass substrate.

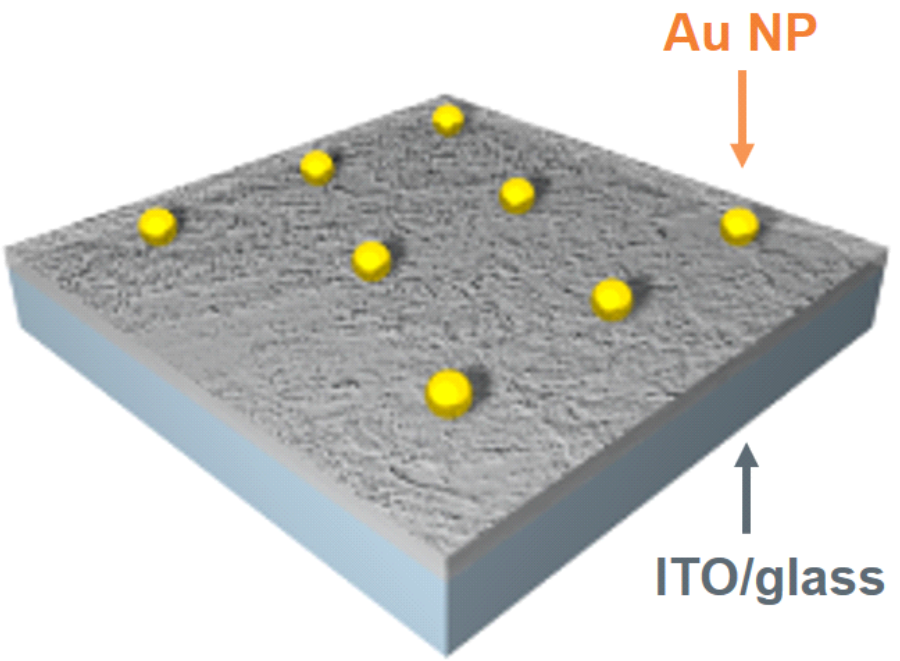

Fig. 2-2 Schematic diagram for fabrication of an array of Au NPs.

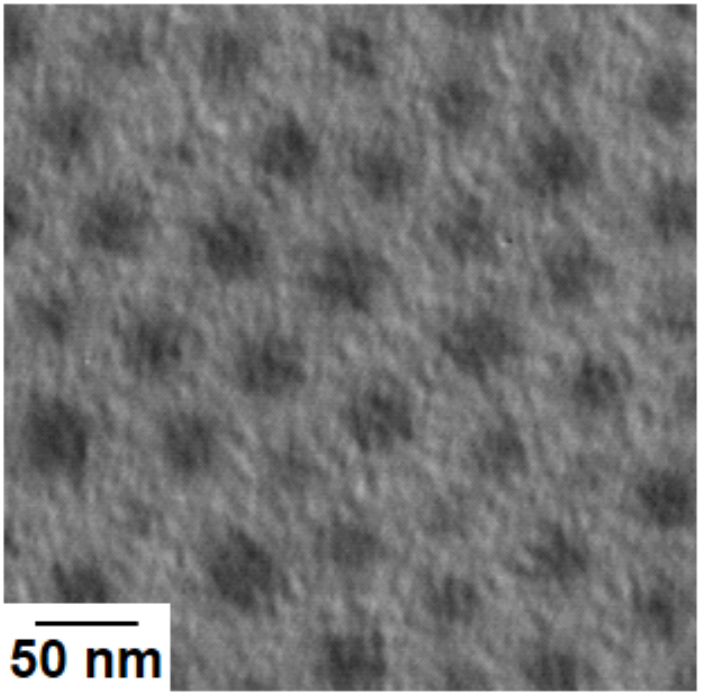

Fig. 2-3 TEM image of a single-layered film of PS-P4VP (51 k-18 k) micelles

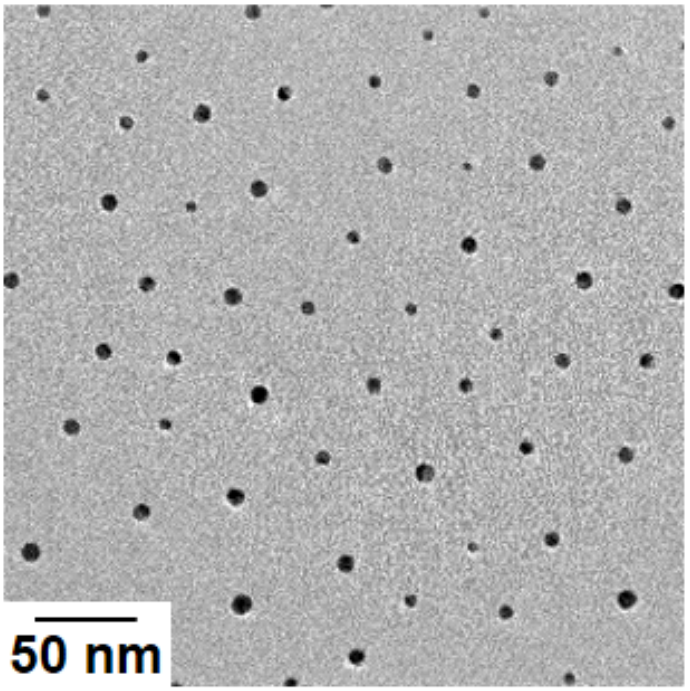

Fig. 2-4 TEM image of Au NP arrays fabricated from PS-P4VP (51 k-18 k)

MW of PS-P4VP	*v* (rpm)	Diameter (nm)	Spacing (nm)	Coverage (*C*, x10^{-5})	Peak potential (V vs NHE)
25 k-7 k	4000	4.5 ± 1.1	27	3.072±0.214	0.909±0.003
32 k-13 k	4000	6.3 ± 0.9	35	4.087±0.293	0.919±0.003
51 k-18 k	2000	7.2 ± 1.3	46	6.704±0.110	0.946±0.002
51 k-18 k	4000	6.8 ± 1.3	51	4.915±0.096	0.938±0.001
48 k-21 k	2000	8.6 ± 1.1	45	7.777±0.454	0.947±0.003

Table 2-1 Information about the arrays of Au NPs aligned on ITO/glass electrode. Spacing of Au NPs was calculated from fast Fourier Transformation (FFT) analyses of corresponding TEM image.

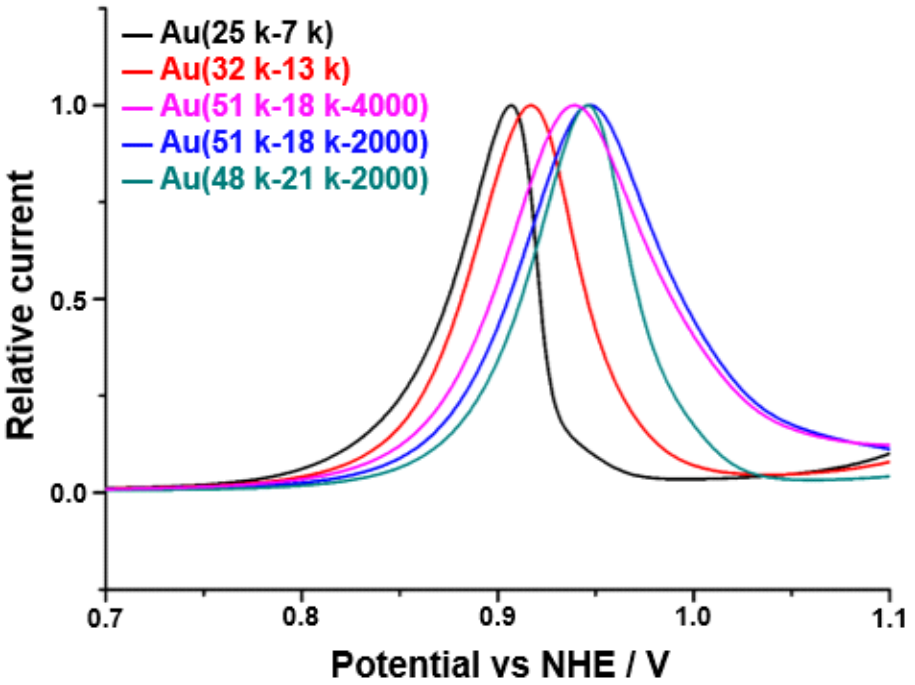

Fig. 2-5 LSVs from arrays of Au NPs on ITO/glass substrate in 10 mM KBr and 0.1 M $HClO_4$ at 5 mVs^{-1}. The currents were normalized by setting the LSVs to have the same oxidation peak current (I_p) for clearer identification of shifts in oxidation peak potential (E_p).

We acquired linear sweep voltammograms (LSVs) to investigate electrochemical oxidation of Au NPs on ITO as prepared. **Fig. 2-5** shows the LSVs of Au NP arrays from five different conditions in **Table 2-1**. For the sake of convenience, Au NPs, which were prepared from PS-P4VP (molecular weight of PS - molecular weight of P4VP-modulated speed of spin-coating), were denoted as Au(molecular weight of PS - molecular weight of P4VP- *v*). Different condition led to different particle diameter and surface coverage as listed in **Table 2-1**. There are two pathways that electrochemical oxidation of the Au in the solution of halide ions can follow.[2, 17]

$$Au^0 + 4Br^- \leftrightarrow AuBr_4^- + 3e^-, E^0 = 0.85\ V\ vs\ NHE$$

$$Au^0 + 2Br^- \leftrightarrow AuBr_2^- + e^-, E^0 = 0.96\ V\ vs\ NHE$$

Upper reaction pathway is known to be thermodynamically preferred[17-19] so that we can assume the faradaic oxidation of three electrons transfer process in the presence of sufficient bromide ions. While there was a report of 1.9 and 1.5 electrons process for this reaction, it could have come from combination of two pathways.[1, 17] By scanning

potential slowly at 5 mVs^{-1}, sufficiently long time was given to make the Au NPs oxidized and dissolved. As seen from the current decay back to the background current, Au NPs were completely dissolved as a consequence of electrochemical oxidation and the charge that flowed during potential scan can be regarded as that for total amount of Au NPs.[1] The amount of charge for faradaic reaction can be calculated by integrating the current under the peak of LSV and was used as surface coverage in this work.

Looking into three conditions from the top in Table 2-1, not only coverage but also diameter of Au NPs are varied to a similar extent with the molecular weight of copolymers, while E_p still shifts. So, the effects of diameter and coverage of Au NPs to the electrochemical reaction are hardly discriminated from each other. Plieth equation allows us to see the influences of diameter to peak potential[4]:

$$E_{NPs} = E_{bulk} - (4\gamma V_m / zFd)$$

where E_{NPs} is the peak potential of electrochemical oxidation of Au NPs, E_{bulk} is the peak potential of bulk Au electrode that was measured to be 1.067 V using Au wafer electrode

under the same condition, γ is the surface stress of Au in vacuum (1880 erg cm^{-2})[4], V_m is molar volume of Au (10.21 cm^3 mol^{-1})[4], F is Faraday constant, d is diameter of NPs and z is the number of electron, which is 3. For the analysis of these experimental results, it is assumed that electrochemical oxidation of Au NPs is that the product of oxidation around NPs affect the oxidation reaction and diffusion layers around Au NPs are overlapped.[1, 3, 7]

Fig. 2-6 shows that experimentally measured E_p (▲) shifted about 0.1 V from the theoretically predicted curve based on Plieth equation (solid line). The experimental results never fit Plieth equation for any z from 1.5 to 3. Interestingly, a constant downward shift of the theoretical curve based on Plieth equation (dashed line) makes itself agree well with the experimentally determined E_p values as depicted in **Fig. 2-6**.

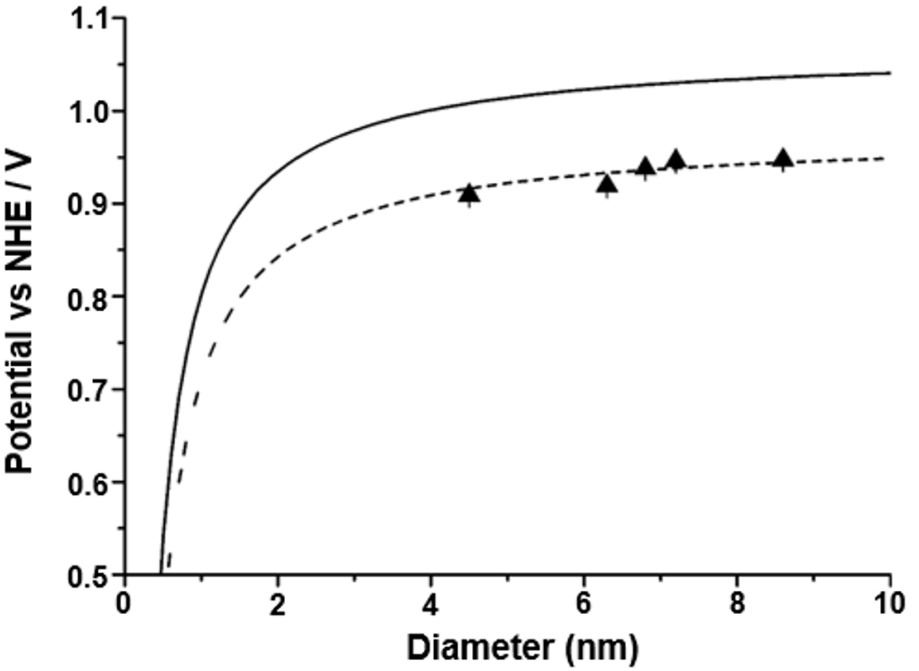

Fig. 2-6 Theoretical E_p as a function of diameter of NPs based on the Plieth equation. Solid line is on the basis of theoretical values assuming that z is 3 and E_p (bulk) is 1.067 V that was measured at an Au wafer. The experimental results (▲) indicate that the Plieth curve shifted to the dashed line (---)

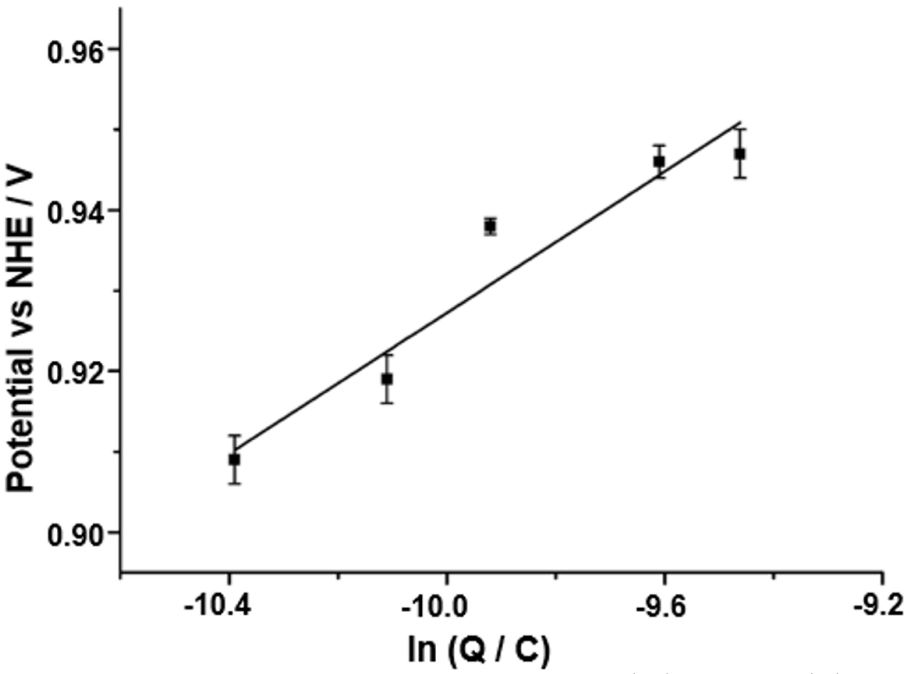

Fig. 2-7 Linear relationship between E_p (■) and ln (Q)

This demonstrates the effect of particle diameter in this system as Plieth relation predicts. More importantly, the significant shifts in E_p cannot be explained by particle diameter, strongly indicating the presence of another factor, which has great influence on electrooxidative dissolution of Au NPs. To seek the key clue for what causes the characteristic shift of E_p, the relationship between E_p and ln (Q) was investigated. **Fig. 2-7** shows that there is a remarkable correlation between E_p shift and coverage, *i.e.* total amount of Au NPs on the substrate. These results show that the coverage is an influential factor for systematic shift of E_p. The same message is found in **Table 2-1** when we compare the results from Au(51 k-18 k-2000) and Au(51 k-18 k-4000). Varying the condition for spin-coating, *v*, with the same molecular weight of diblock copolymer, we can prepare a pair of Au NPs arrays where the coverages are markedly different while the particle diameters are similar within the standard deviations. E_p of Au(51 k-18 k-4000) is negatively shifted compared to Au(51 k-18 k-2000). On the other hand, Au(48 k-21

k−2000) has significantly larger particles in diameter than Au(51 k−18 k−2000), *i.e.* out of the standard deviations, whereas this pair have much less difference in coverage compared with Au(51 k−18 k−2000) and Au(51 k−18 k−4000). In spite of the obvious discrepancy in particle diameter, Au(48 k−21 k−2000) and Au(51 k−18 k−2000) give almost same E_p. This result shows that the coverage of NPs is more influential factor than diameter under the condition that the oxidized species concentration near the Au NPs affects the oxidation reaction and diffusion layers that are overlapped.

2.4 Conclusion

In summary, we prepared the arrays of Au NPs that had finely tuned diameter and inter-particle spacing without aggregation. There was no adlayer that could influence on electrochemical response on the nanoparticle arrays, creating the condition under which the gold ion concentration near the Au NPs affect the oxidation reaction and diffusion layer overlapped electrode system. Stripping voltammetry from such sophisticatedly controlled electrodes provided the quantitative information about the influence of diameter and coverage on peak potential of electrochemical oxidation.

Coverage, total amount of Au on the substrate, is more influential than diameter on the oxidation potential. This can be extended to an implication that stability of metal NPs is seriously affected by amount of the metal on the substrate. The result from the present work confirms the fact that high coverage of NPs is more stable while low coverage is favourable for cost. This has been obscure because there has been no study with as precisely controlled NPs arrays

as the present system before. In terms of designing nanoparticle-based electrocatalysts, the lesson is that catalytic power should be considered most seriously to select particle diameter as long as the amount of metals securing stability.

2.5 References

[1] Ivanova, O. S., Zamborini, F. P., *Anal. Chem.,* **2010**, *82*, 5844.

[2] Masitas, R. A., Zamborini, F. P., *J. Am. Chem. Soc.,* **2012**, *134*, 5014.

[3] Toh, H. S., Batchelor-McAuley, C., Tschulik, K., Uhlemann, M., Crossley, A., Compton, R. G., *Nanoscale,* **2013**, *5*, 4884.

[4] Plieth, W. J., *J. Phys. Chem.,* **1982**, *86*, 3166.

[5] Henglein, A., *J. Phys. Chem.,* **1993**, *97*, 5457.

[6] Brainina, K. Z., Galperin, L. G., Galperin, A. L., *J. Solid State Electrochem.,* **2010**, *14*, 981.

[7] Ivanova, O. S., Zamborini, F. P., *J. Am. Chem. Soc.,* **2010**, *132*, 70.

[8] Tang, L., Han, B., Persson, K., Friesen, C., He, T., Sieradzki, K., Ceder, G., *J. Am. Chem. Soc.,* **2010**, *132*, 596.

[9] Tang, L., Li, X., Cammarata, R. C., Friesen, C., Sieradzki, K., *J. Am. Chem. Soc.,* **2010**, *132*, 11722.

[10] Del Popolo, M., Leiva, E., Kleine, H., Meier, J., Stimming, U., Mariscal, M., Schmickler, W., *Appl. Phys. Lett.,*

2002, *81*, 2635.

[11] Kolb, D. M., Engelmann, G. E., Ziegler, J. C., *Angew. Chem. Int. Ed.,* 2000, *39*, 1123.

[12] Ward Jones, S. E., Chevallier, F. G., Paddon, C. A., Compton, R. G., *Anal. Chem.,* 2007, *79*, 4110.

[13] Jones, S. E. W., Campbell, F. W., Baron, R., Xiao, L., Compton, R. G., *J. Phys. Chem. C,* 2008, *112*, 17820.

[14] Jones, S. E. W., Toghill, K. E., Zheng, S. H., Morin, S., Compton, R. G., *J. Phys. Chem. C,* 2009, *113*, 2846.

[15] Yun, S.-H., Yoo, S. I., Jung, J. C., Zin, W.-C., Sohn, B.-H., *Chem. Mater.,* 2006, *18*, 5646.

[16] Kim, S.-S., Kim, Y.-R., Chung, T. D., Sohn, B.-H., *Adv. Funct. Mater.,* 2014, *24*, 2764.

[17] Zhou, Y. G., Rees, N. V., Pillay, J., Tshikhudo, R., Vilakazi, S., Compton, R. G., *Chem. Commun.,* 2012, *48*, 224.

[18] Kolics, A., Thomas, A. E., Wieckowski, A., *J. Chem. Soc., Faraday Trans.,* 1996, *92*, 3727.

[19] Diaz, M. A., Kelsall, G. H., Welham, N. J., *J. Electroanal. Chem.,* 1993, *361*, 25.

3. In situ Confocal Microscopy of Electrochemical Generation and Collision of Emulsion Droplets in Bromide Redox System

3.1 Introduction

Emulsion droplets have been an interesting research theme for various aspects in industrial processes. What we can access to investigate droplets is mostly ensemble properties. Lack of proper analytical methods to characterize individual particles is the cause of such limited knowledge about them. In this regard, 'particle-impact chronoamperometry' is getting a new spotlight recently.[1, 2] This technique is a simple but informative way to detect electrochemical signals originated by individual particles.[1] In the presence of particles near the electrode, chronoamperometry typically gives current spikes[3], which are current surges that happen when the particles contact the electrode surface[2]. Such current spikes contain information about size[3],

concentration[4], and aggregation state[5] of the particles and electron transfer associated with them[6-8]. This method is applied to study of, not only metal nanoparticles but also 'soft particles', such as liposomes[9-12], viruses[13], single macromolecules[14] and emulsion droplets containing redox species[15-17].

1-methyl-1-ethylpyrrolidinium bromide (MEPBr) is one of quaternary ammonium bromides (QBr's) widely used in redox flow batteries (RFBs)[18-21]. It captures electrochemically produced bromine (Br_2), during electro-oxidation of Br^-, to induce the formation of insoluble organic emulsion droplets of $MEPBr_3$. Formation of such emulsion prevents from permeation through the battery membrane and self-discharging of electrogenerated Br_2, which is one of the key causes bringing about malfunction of RFB systems.[22-28] Reportedly, $MEPBr_3$ droplets participate in Br^- electrooxidation rather than behaving merely as bromine complexing agents[29], making the system even more complex. The electrochemistry involving MEPBr and $MEPBr_3$, however, remains unknown. For

instance, it is still unclear what causes the characteristic spikes in chronoamperograms although it is assumed that a spike appears when a droplet collides with the electrode surface and whether the $MEPBr_3$ emulsions are homogenously created in aqueous solution or heterogeneously formed on the electrode. In addition, it is unknown why the oxidative current of MEPBr is larger than currents from aqueous Br^- oxidation without MEP^+.

In this study, we investigate the electro-oxidation of Br^- in $MEPBr_3$ droplet through comparison between electrochemical analysis and *in-situ* confocal microscopy. Previous reports showed collision events of particles such as nanoparticles, fluorescent beads and some soft particles through fluorescence[30, 31] and plasmonic signals[32-36] that are produced when particles collide with the electrode. Unfortunately, it is difficult to directly observe the generation and behavior of particles in the solution. This led us to seek an alternative way of observing the $MEPBr_3$ droplets, *i.e.* by using *in-situ* confocal microscopy. Droplets are predicted to be a few μm in diameter, for which

confocal microscopy can provide direct optical images with sufficient resolution. The optical images can show the change in droplets at the focused range used. Using cylindrical wire electrode helps with monitoring the stereoscopic movement of droplet and ultramicroelectrode (UME) giving low background current suits for simultaneous acquisition of the optical images and transient current caused by a droplet collision moment. Therefore, *in-situ* confocal microscopy allows us to see directly generation, diffusion, and collision of the droplets at the electrode, and how they change as potential varies. These are expected to provide a better understanding of the contribution of $MEPBr_3$ droplets to the oxidation of Br^- in redox flow batteries.

3.2 Experimental

3.2.1. Materials and reagents

1-ethyl-1-methylpyrrolidinium bromide and potassium bromide were acquired from Sigma-Aldrich. Sulfuric acid (95%) and potassium sulfate were purchased from Deajung and Alfa Aesar, respectively. All the aqueous solutions in these experiments were prepared with ultrapure deionized water produced by a Barnstead Nanopure system from Thermo Scientific.

3.2.2. Electrochemical measurements

Cyclic voltammograms and chronoamperograms were obtained with a CHI 750 electrochemical workstation from CHI instruments. The electrochemical cell consisted of three electrodes. The working electrodes were either a Pt UMEs (diameter: d = 10 μm) or a Pt microwire electrode (diameter: d = 25 μm). A silver/silver chloride (3 M

potassium chloride) and a Pt wire were used as reference and counter electrode, respectively. The pH of the solutions comprising 0.5 M potassium sulfate and 1-ethyl-1-methylpyrrolidinium bromide or potassium bromide, was adjusted with sulfuric acid.

3.2.3. Confocal microscopy imaging

Imaging was carried out with a Zeiss LSM880 confocal laser scanning microscope equipped with a laser argon-multiline for RGB and a water-immersion objective (20x, N.A. = 1.0; Zeiss). Series of images were acquired with the interval of about 15 ~ 150 ms and were sharpened to clearly see the shape and movement of the droplet using a ZEN (black edition; Zeiss) software.

3.3 Results and Discussion

The homogeneous complexation process of $MEPBr_3$ proposed in the literature is represented as follows.[29]

$$Br_3^- + 2e^- \leftrightarrow 3Br^- \quad (1)$$

$$MEP^+ + Br_3^- \leftrightarrow MEPBr_3 \quad (2)$$

This suggested mechanism proposes that Br_3^-, which is generated on the electrode surface in reaction (1), encounters the 1-methyl-1-ethylpyrrolidinium cation, MEP^+, to form a complex homogeneously, $MEPBr_3$, as described in reaction (2). This is supported by *in-situ* FT-IR investigations[26, 27]. Multiple insoluble $MEPBr_3$ complexes agglomerate themselves to create a droplet in the aqueous solution. When the droplet hanging around the solution happens to reach the electrode surface, additional spike current is produced in voltammograms and chronoamperograms. From the electrochemical analysis and simulation study in $MEPBr_3$ droplet, it was predicted that Br^- is enriched *ca.* 7.5M in the droplet and causes the spike

current.[29, 37] This is a proposed scenario, although highly probable as implied by a couple of indirect observations, which has not been proved by direct imaging and thereby the respective steps of the previously mentioned mechanism remains veiled to date.

To address this issue, we introduce confocal microscopy to monitor what occurs at the electrode during the electrochemical measurements. Fig. 3-1 and 3-2 shows the experimental scheme for simultaneous measurements using a potentiostat and a confocal microscope. Three electrodes, including a Pt wire or a UME as working electrodes, constitute the electrochemical system installed on the mount of an upright type confocal microscope.

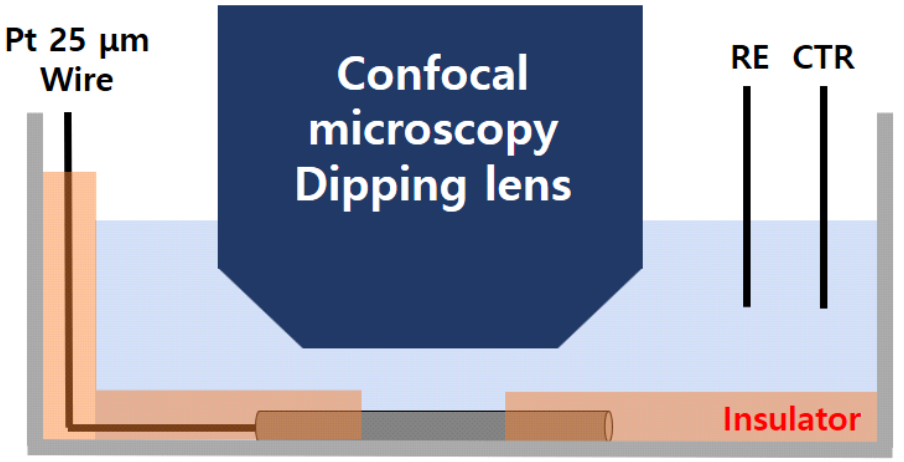

Fig. 3-1 Schematic diagram of electrochemical measurement and confocal imaging. Pt wire (25 μm in diameter) insulated except the part exposed to the electrolyte (ca. 2.5 mm long)

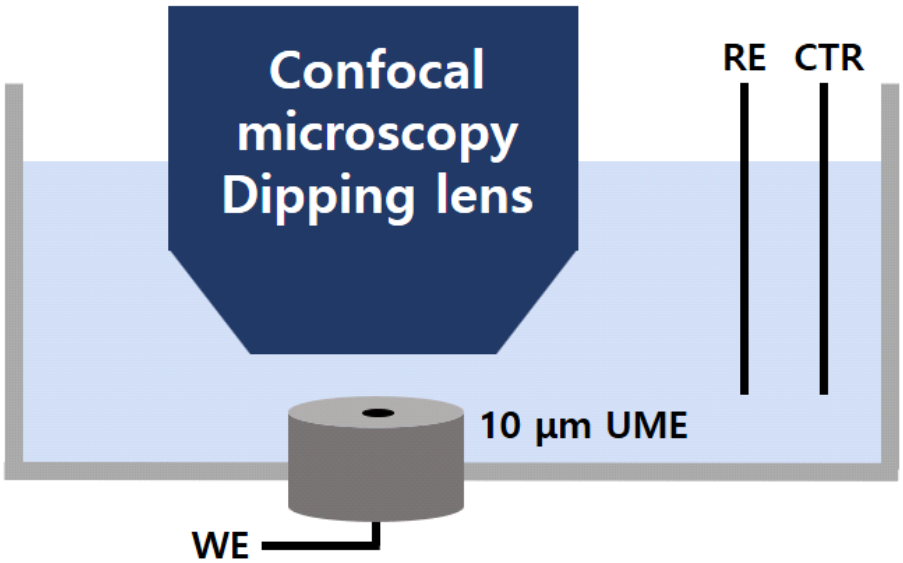

Fig. 3-2 Schematic diagram of electrochemical measurement and confocal imaging. Pt UME (10 μm in diameter) utilized in electrochemical cell

The Pt wire of 25 μm in diameter provides a cylindrical electrode where its length exposed to the solution is about 2.5 mm. (**Fig. 3-3**) This wire electrode helps see the stereoscopic movement of droplets through the images in both vertical and horizontal views from the electrode surface. (**Fig. 3-4 and 3-5**) Its large surface area leads to correspondingly high background current in the current transient curve and the cyclic voltammogram so that it is difficult to observe distinct spikes clearly. UME is a good solution to this problem (**Fig. 3-2**). It allows discrimination of discrete current spikes at a constant potential as to investigate whether droplet collision and current spike coincide with each other. The UME was modified to be installed on a confocal microsocopy. (**Fig. 3-6**) An objective lens immersed in solution enables clean optical high-resolution images to be obtained. The dipping lens is sufficiently stable within the pH range between 5 and 8. For this reason, the supporting electrolyte solution is used 0.5 M K_2SO_4 solution at pH 5.1.

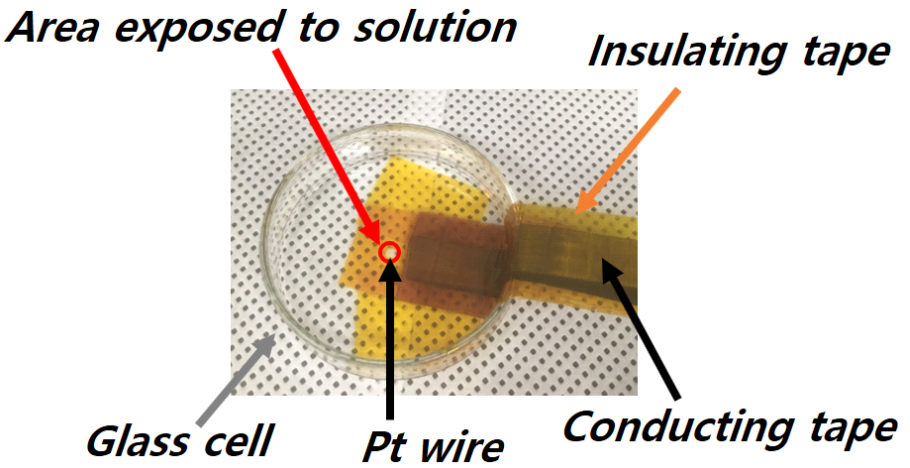

Fig. 3-3 Electrochemical cell using Pt wire as working electrode

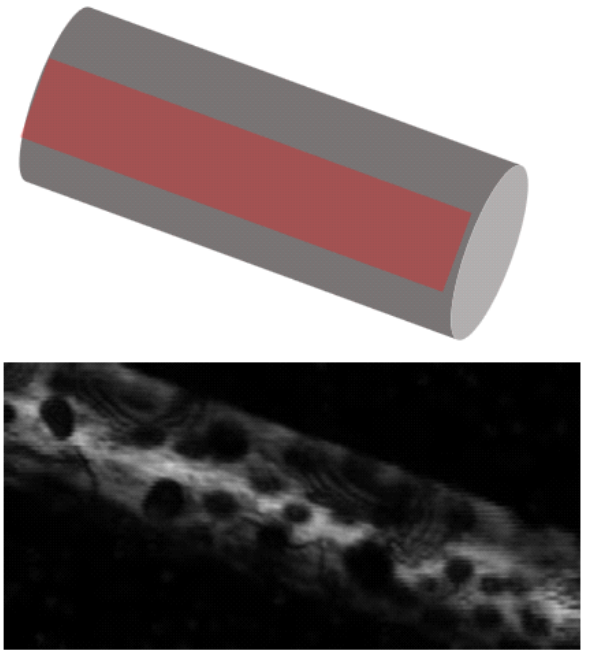

Fig. 3-4 The focus is on the uppermost surface of the cylindrical wire electrode. The upper scheme is the planes focused (red box) and the lower is actual image at 1.0 V.

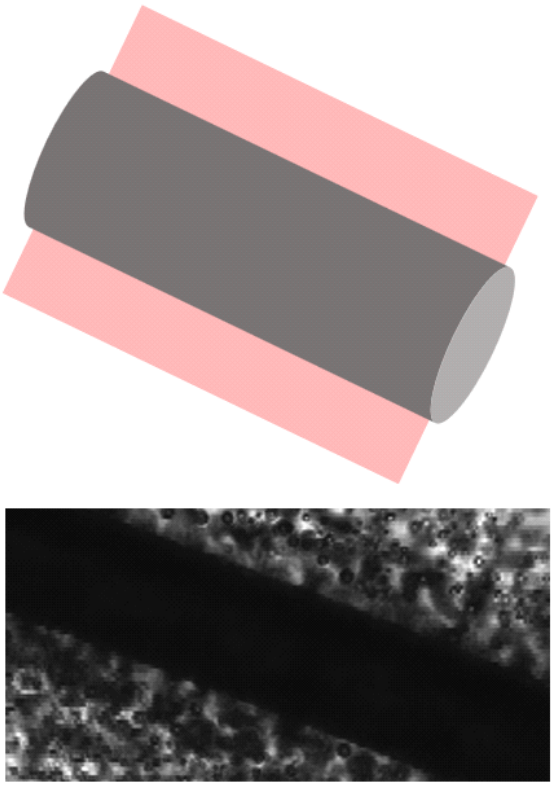

Fig. 3-5 The focus is on a plane perpendicular to the sideward electrode surface. The upper scheme is the planes focused (red box) and the lower is actual image at 1.0 V.

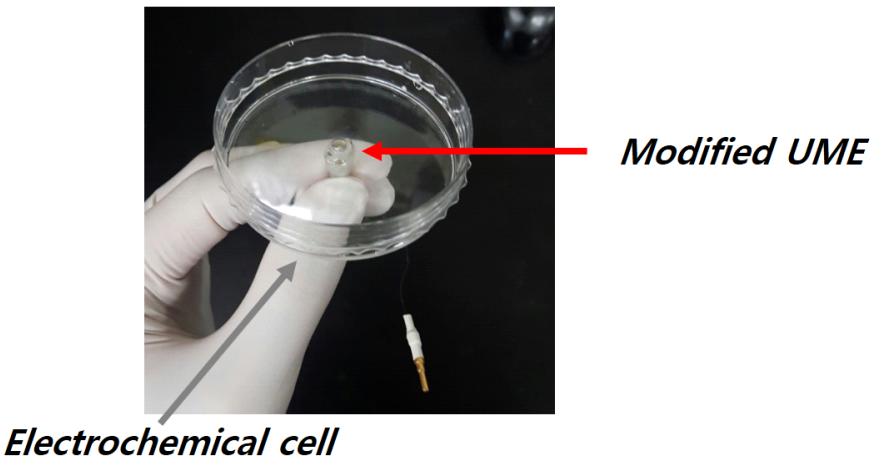

Fig. 3-6 Electrochemical cell using UME as working electrode

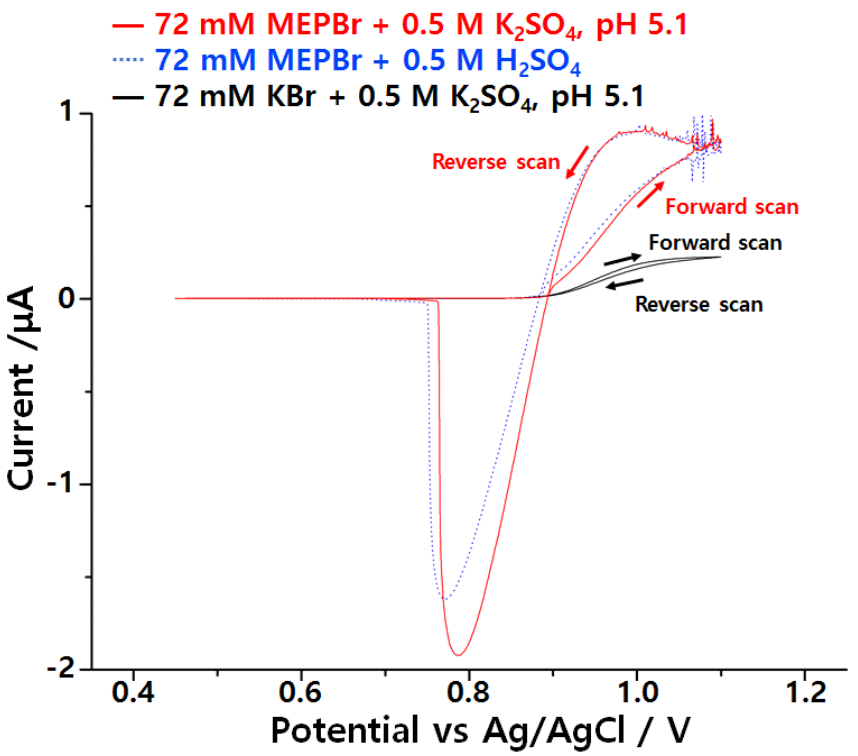

Fig. 3-7 Cyclic voltammograms recorded in 72 mM MEPBr + 0.5 M K_2SO_4 at pH 5.1 (red line), 72 mM KBr + 0.5 M K_2SO_4 solution at pH 5.1 (black line) and 72 mM MEPBr + 0.5 M H_2SO_4 (blue dotted line). A Pt UME was used as working electrode and scan rate was 10 mV s^{-1}.

Fig. 3-7 shows the influences of MEP^+ and pH to the electrochemical redox behavior of Br^-. The cyclic voltammogram of 72 mM aqueous KBr at pH 5.1 (black line) tells that sufficiently high overpotential gives rise to diffusion-controlled Br^- oxidation at the Pt UME in the absence of MEP^+. The faradaic current is smaller than that in the presence of MEP^+ and no spike appears. A 72 mM aqueous MEPBr at pH 5.1 (red line) starts giving oxidation current at around 0.85 V and reaches diffusion-controlled state at a potential higher than 1.0 V. Overall oxidative current is larger than that of KBr solution, and current spikes randomly. At the same potential, the current during the reverse scan is much larger than that during the forward one, indicating that the redox process is not a simple diffusion system. This implies that the products of electrochemical oxidation accumulate on the electrode to accelerate further oxidation rather than blocking reactant diffusion towards the electrode. Unlike KBr, MEPBr solution undergoes reduction in the reverse scan. The reduction peak would be correlate with the reduction of Br_3^- in droplets

adsorbed on the electrode.[23] The area of the reduction peak is proportional to the total charge for oxidation. However, the charge of oxidation is 1.4 times larger than the amount of reduction charge. This tells that all of the oxidized species do not come back to the electrode. At low pH, the voltammetric changes a little without significant difference on the whole as shown the voltammogram from the solution of 72 mM MEPBr and 0.5 M H_2SO_4 (blue dotted line).

In order to further assess the fundamental electrochemical behavior of this system, we examine the Pt wire electrode system in the potential range of 0.8 to 1.0 V by confocal microscopy. The cyclic voltammogram of Pt wire electrode is shown in **Fig. 3-8**. Neither oxidation current nor droplet is observed at 0.8 V. (**Fig. 3-9**) At 0.85 V, when the oxidation current begins to increase, small droplets start appearing and merging into larger ones on the electrode surface. (**Fig. 3-10**) Since the chemically synthesized $MEPBr_3$ droplets have brownish color[29], the droplets in the confocal images appear black. The droplets keep growing as the potential

increases, and are still adhered to the electrode surface. At 0.925 V, small droplets are generated on the electrode surface and are released to the bulk solution. Some droplets, adsorbed on the surface of the electrode, gradually aggregate themselves to form a larger hemispherical one. Detached droplets are much smaller than the droplets still attached to the surface. (**Fig. 3-11**) Upon higher overpotential, the size of the droplets attached to the electrode surface decreases and a greater number of droplets leave the surface to the bulk solution. On the electrode surface at 1.0 V, it is even hard to see growth of droplets. Rather, small droplets quickly emerge and some of them aggregate in the solution, not on the very electrode surface. (**Fig. 3-12**) The emulsion consists of extremely small droplets with a haze-like appearance. Interestingly, a few droplets hovering over the electrode surface move back to the surface. In order to understand why the droplets move back to the electrode again and collides, we compared the size of the droplets hovering over the electrode surface (**lower image of Fig. 3-12**) with the size of those diffusing away from the

electrode (**upper image of Fig. 3-12**). 20 droplets hovering over are 3.20 ± 0.84 μm in diameter. For 30 droplets diffusing away from the electrode surface, the diameters are 1.84 ± 0.51 μm. The UME, which is immersed inversely in the solution, *i.e.* facing downward, shows no significant change in the number or shape of the spikes due to collisions of droplets. Therefore, it is improbable that weight of droplet is responsible for collision with the electrode. Confocal microscopic images tell that electrogenerated droplets randomly move and hit others. (**Fig. 3-13, 14 and 15**) Stochastic collisions among droplets appear to make them drift in arbitrary directions. As a consequence, some of the droplets contact the electrode surface to produce spikes.

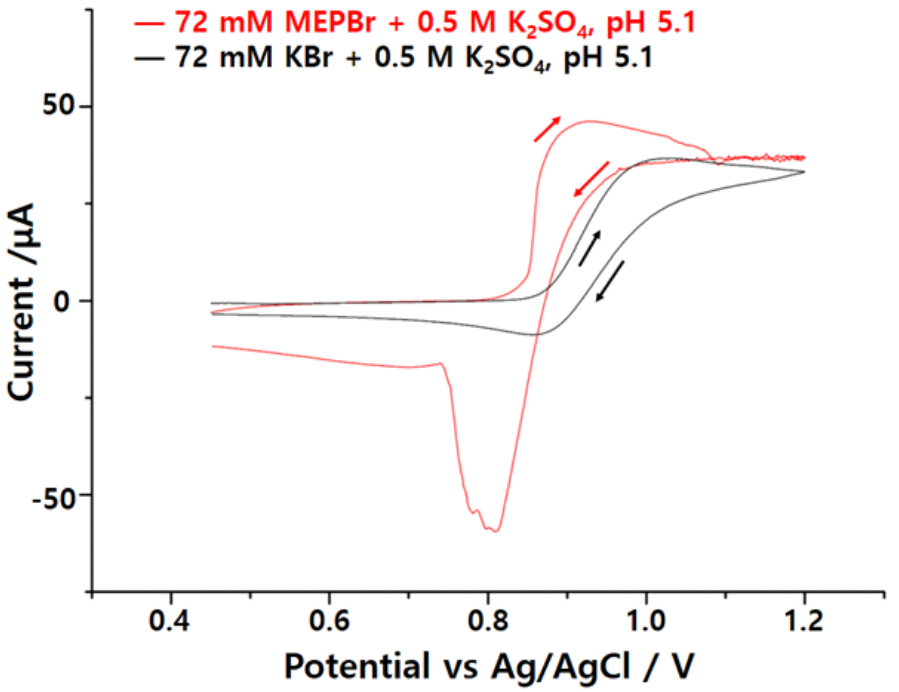

Fig. 3-8 Cyclic voltammograms recorded in 72 mM MEPBr + 0.5 M K_2SO_4 at pH 5.1 (red line) and 72 mM KBr + 0.5 M K_2SO_4 solution at pH 5.1 (black line). A 25 μm Pt wire was used as working electrode and scan rate was 10 mV s^{-1}.

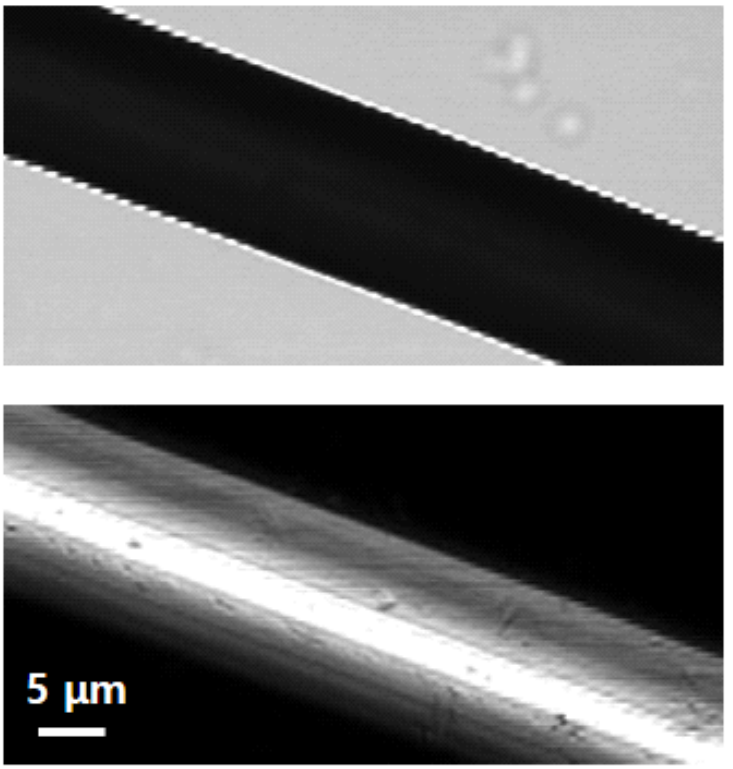

Fig. 3-9 Confocal images taken 15 s after 0.8 V potentials to Pt wire electrode in 72 mM MEPBr + 0.5 M K_2SO_4 at pH 5.1.

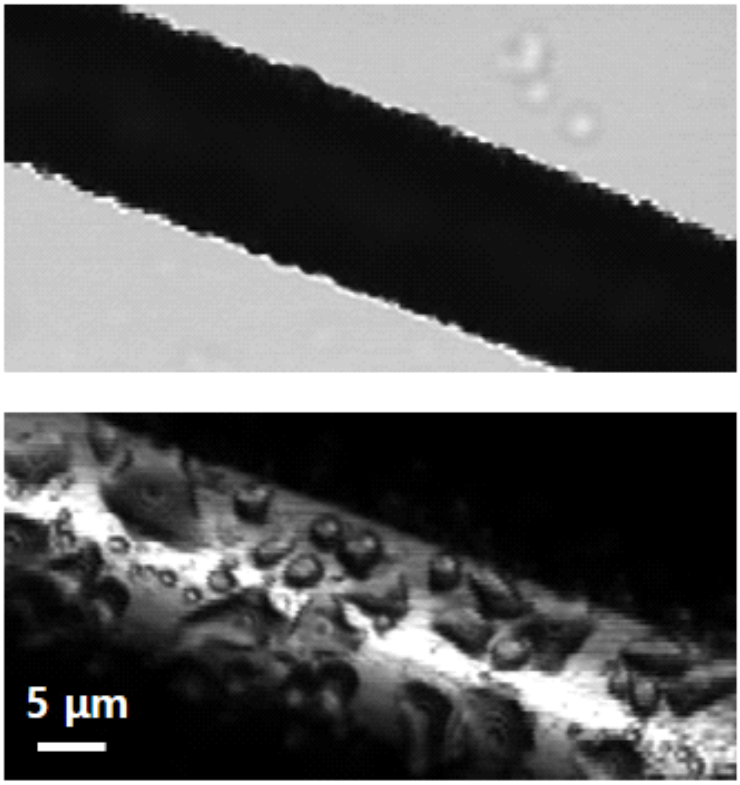

Fig. 3-10 Confocal images taken 15 s after 0.85 V potentials to Pt wire electrode in 72 mM MEPBr + 0.5 M K_2SO_4 at pH 5.1.

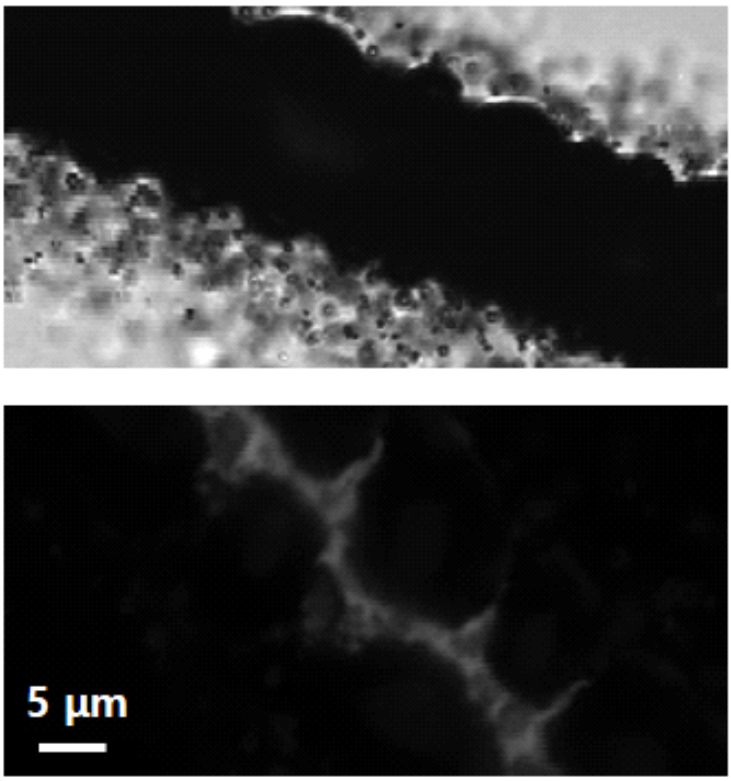

Fig. 3-11 Confocal images taken 15 s after 0.925 V potentials to Pt wire electrode in 72 mM MEPBr + 0.5 M K_2SO_4 at pH 5.1.

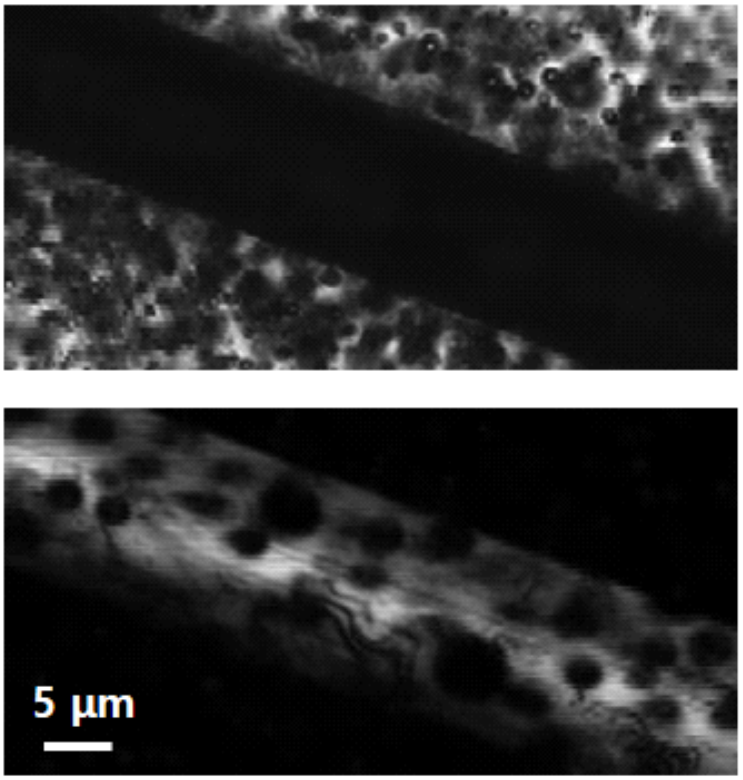

Fig. 3-12 Confocal images taken 15 s after 1.0 V potentials to Pt wire electrode in 72 mM MEPBr + 0.5 M K_2SO_4 at pH 5.1.

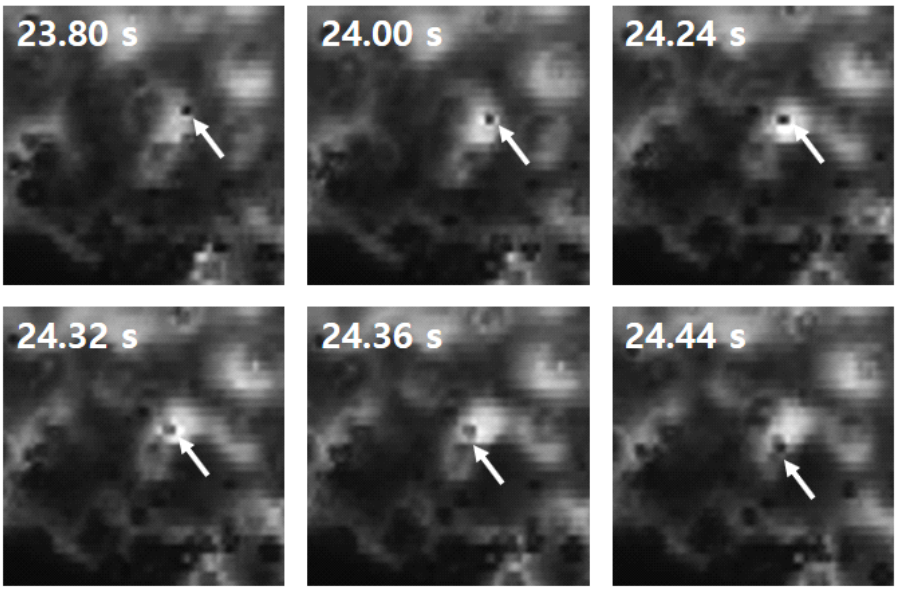

Fig. 3-13 The images tracing a droplet that approaches the electrode surface as a function of time. The targeted droplet (indicated by and a white arrow) as time elapses since 1.0 V was applied.

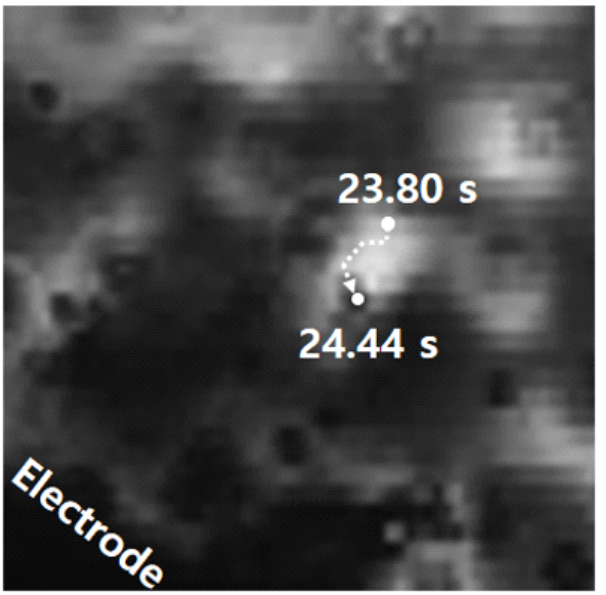

Fig. 3-14 The images tracing a droplet that approaches the electrode surface as a function of time. Trajectory of the droplet from 23.80 s to 24.44 s

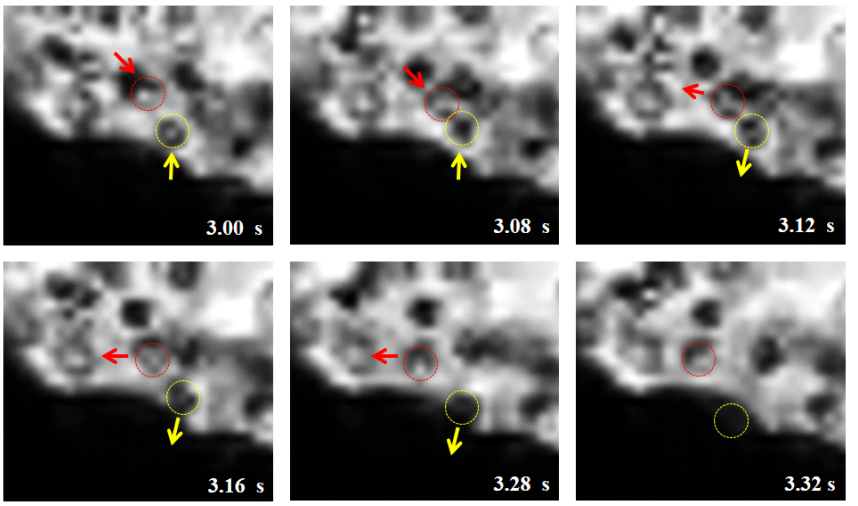

Fig. 3-15 The images tracing droplets that approach the electrode surface as a function of time. The targeted droplets (indicated by yellow and red circles) as time elapses at 0.925 V applied. They drift in random direction that is switched by collision with another droplet.

Fig. 3-16 shows magnifications of the images of Fig. 12, focused at 1 μm distance range from the electrode surface. Thus, the droplets in these images are located very close to the electrode. These droplets are not adsorbed on the electrode surface but seem to drift over it (Fig. 3-16a). As soon as a droplet collides with the electrode, it spreads out over the surface (Fig. 3-16b) and becomes flat to adhere to the surface in 0.06 s (Fig. 3-16c). Thereafter, the droplet on the electrode gradually fades away to become a hazy shape(Fig. 3-16d, e and f). Presumably, the droplet disintegrates in miniscule pieces. There are other examples of similar events when droplets collide with the Pt wire electrode surface. (Fig. 3-17 to 20)

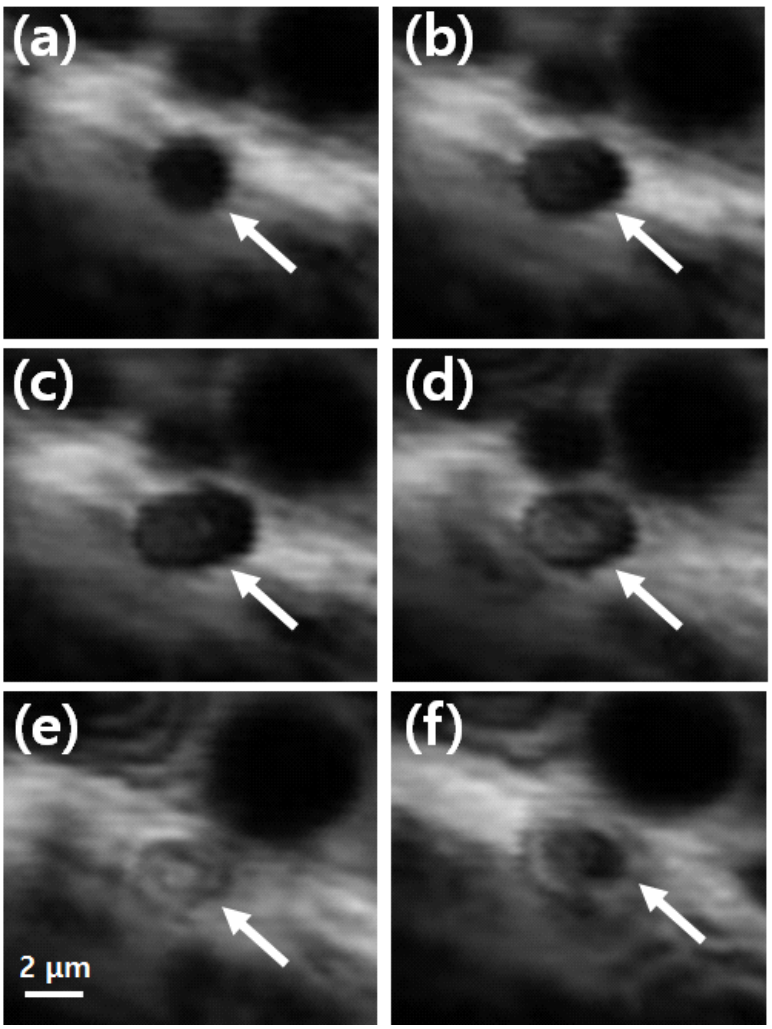

Fig. 3-16 Images at the moment the emulsion collides with surface of a Pt wire electrode. White arrows indicate the position of the targeted droplet. The time elapsed at 1.0 V (a) 16.96 s, (b) 16.99 s, (c) 17.02 s, (d) 17.62 s, (e) 18.04 s, (f) 18.34 s, respectively. Scale bar = 2 μm

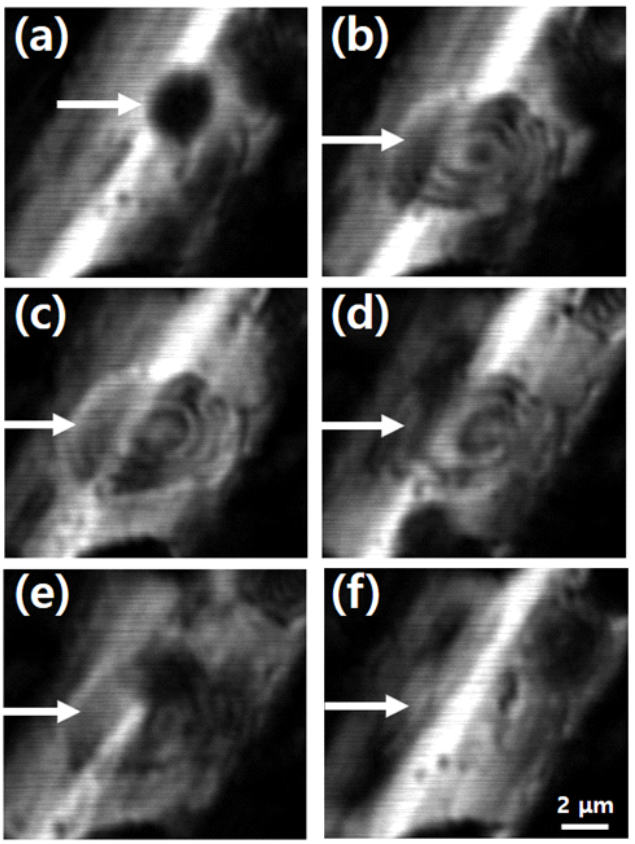

Fig. 3-17 Images at the moment the emulsion collides with the surface of a Pt wire electrode. White arrows indicate the position of the targeted droplet. 1.0 V was applied to the electrode. The entire images, out of which 6 images were selected, were collected at intervals of 0.15 s. The time from the first image is (a) 0 s, (b) 0.15 s, (c) 0.45 s, (d) 1.35 s, (e) 1.95 s, (f) 3.60 s, respectively. Scale bar = 2 μ m.

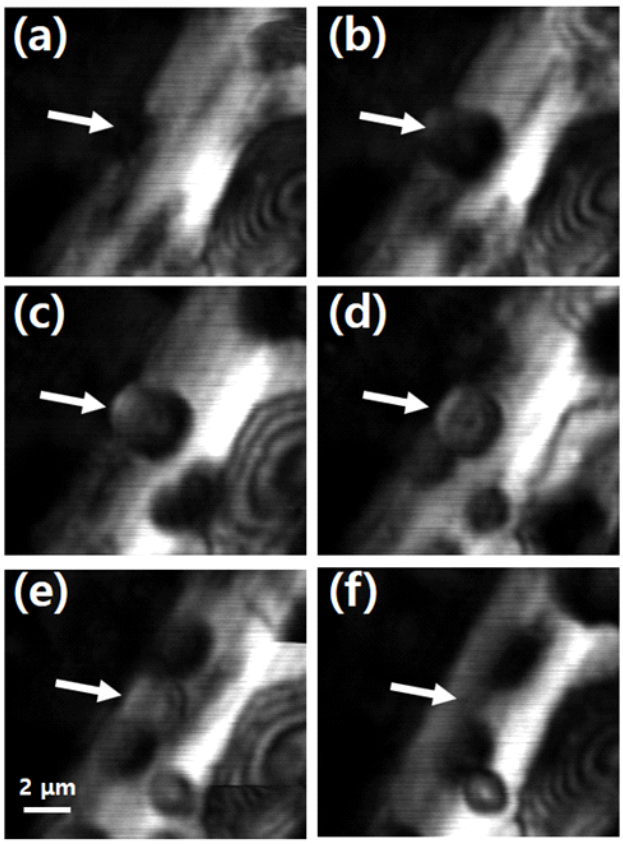

Fig. 3-18 Images at the moment the emulsion collides with the surface of a Pt wire electrode. White arrows indicate the position of the targeted droplet. A 1.0 V was applied to the electrode. The entire images, out of which 6 images were selected, were collected at intervals of 0.15 s. The time from the first image is (a) 0 s, (b) 0.15 s, (c) 1.35 s, (d) 2.10 s, (e) 2.40 s, (f) 3.00 s, respectively. Scale bar = 2 μ m.

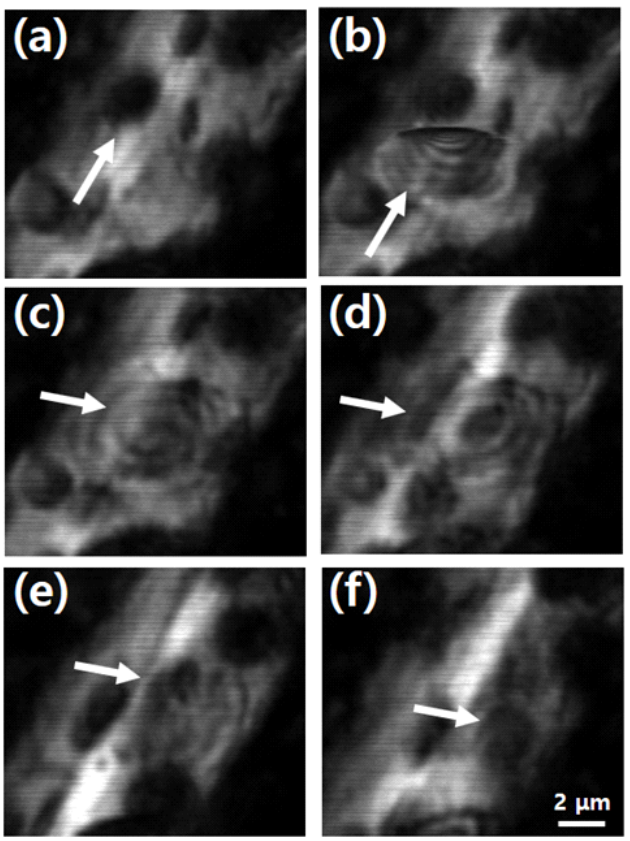

Fig. 3-19 Images at the moment the emulsion collides with the surface of a Pt wire electrode. White arrows indicate the position of the targeted droplet. A 1.0 V was applied to the electrode. The entire images, out of which 6 images were selected, were collected at intervals of 0.15 s. The time from the first image is (a) 0 s, (b) 0.15 s, (c) 0.30 s, (d) 0.60 s, (e) 1.35 s, (f) 2.25 s, respectively. Scale bar = 2 μ m.

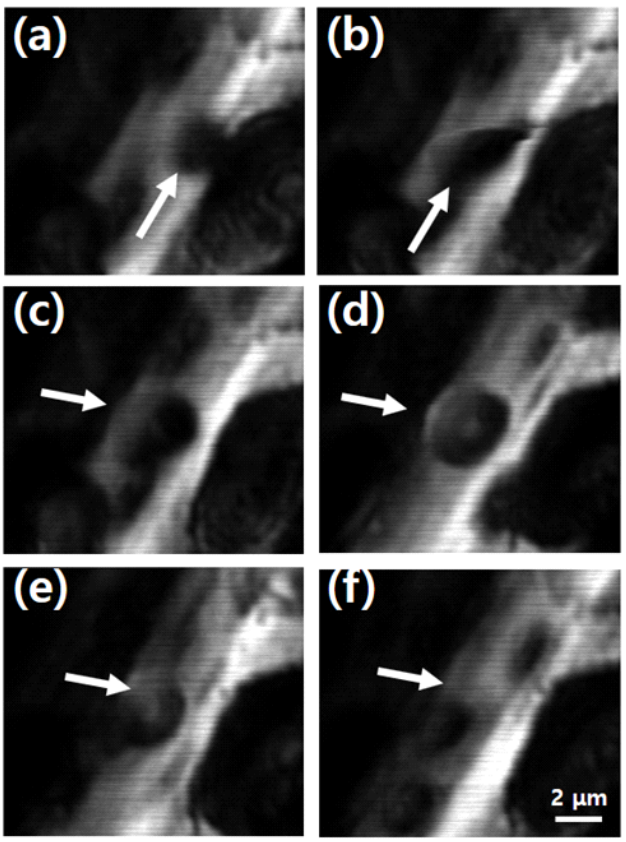

Fig. 3-20 Images at the moment the emulsion collides with the surface of a Pt wire electrode. White arrows indicate the position of the targeted droplet. A 1.0 V was applied to the electrode. The entire images, out of which 6 images were selected, were collected at intervals of 0.15 s. The time from the first image is (a) 0 s, (b) 0.15 s, (c) 0.30 s, (d) 2.70 s, (e) 3.45 s, (f) 4.05 s, respectively. Scale bar = 2 μ m.

The collision in confocal microscopic images is observed at potentials above 1.0 V. This is same as the potential range where the characteristic spikes appear in the corresponding cyclic voltammograms in **Fig. 3-7**. The current transient curves of a Pt UME of 10 μm diameter, which produces a lower background current than the Pt wire electrode, allow us to demonstrate that the droplet collisions cause the current spikes. **Fig. 3-21** shows the chronoamperogram of 32 mM MEPBr diluted with 0.5 M K_2SO_4 at pH 5.1 and 1.0 V. Dilution of the solution makes the number of spikes small enough to compare the confocal microscopic images with individual spikes in the current transient curve, which were simultaneously acquired. The red dots in **Fig. 3-21** indicate the droplets collision time with the electrode, which are determined based on the confocal microscopic images continuously taken. In **Fig. 3-21**, successive droplet collision starting at 20.21 seconds are shown in **Fig. 3-22 and 23**. The elapsed times of red dots from the images coincide with the spikes on the chronoamperogram as seen in **Fig. 3-21**. Some spikes observed in the chronoamperogram, however,

are invisible under the microscope. Smaller spikes following immediately after a large one, *e.g.* at 22.24 s, are not visible in the confocal microscopy images. For a large spike, corresponding collided droplet covers a wide, sometimes even entire, area of the electrode so that the whole image appears entirely black and it is not possible to see small spots (**Fig. 3-24**).

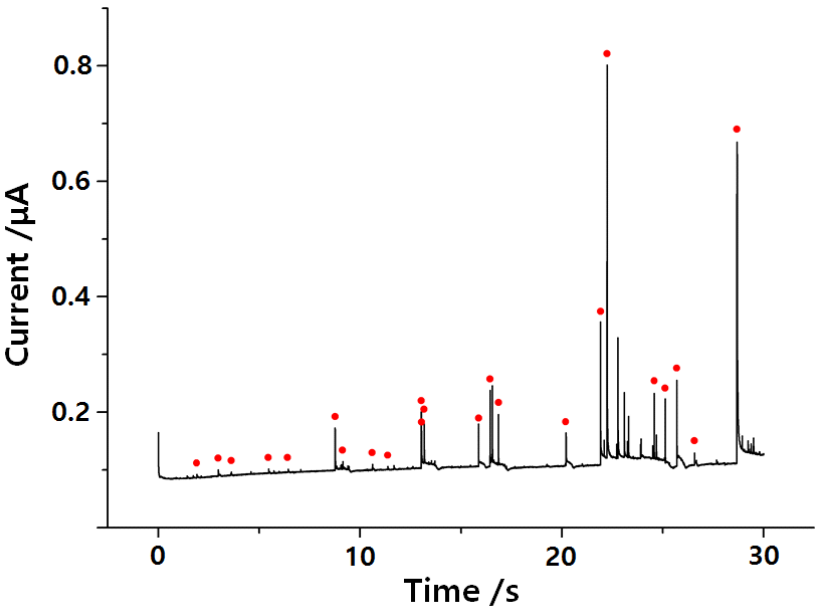

Fig. 3-21 Chronoamperogram from a Pt UME monitored by confocal microscopy. (black line) Red dots are the moments droplets collide with the electrode surface.

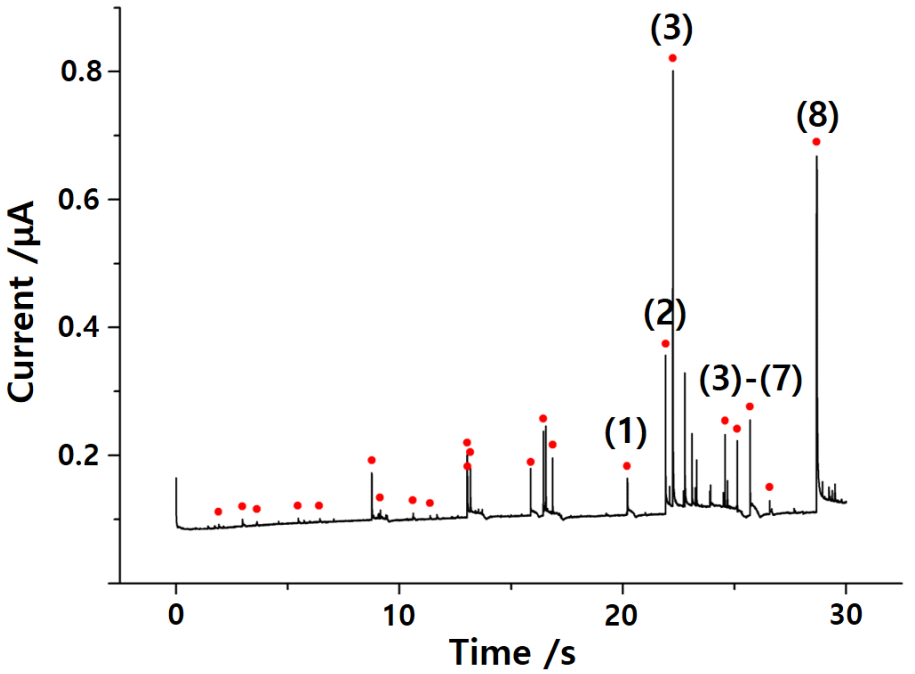

Fig. 3-22 Chronoamperogram from a Pt UME monitored by confocal microscopy. (black line) Red dots are the moments droplets collide with the electrode surface. Succeeding spike current is marked by series of number.

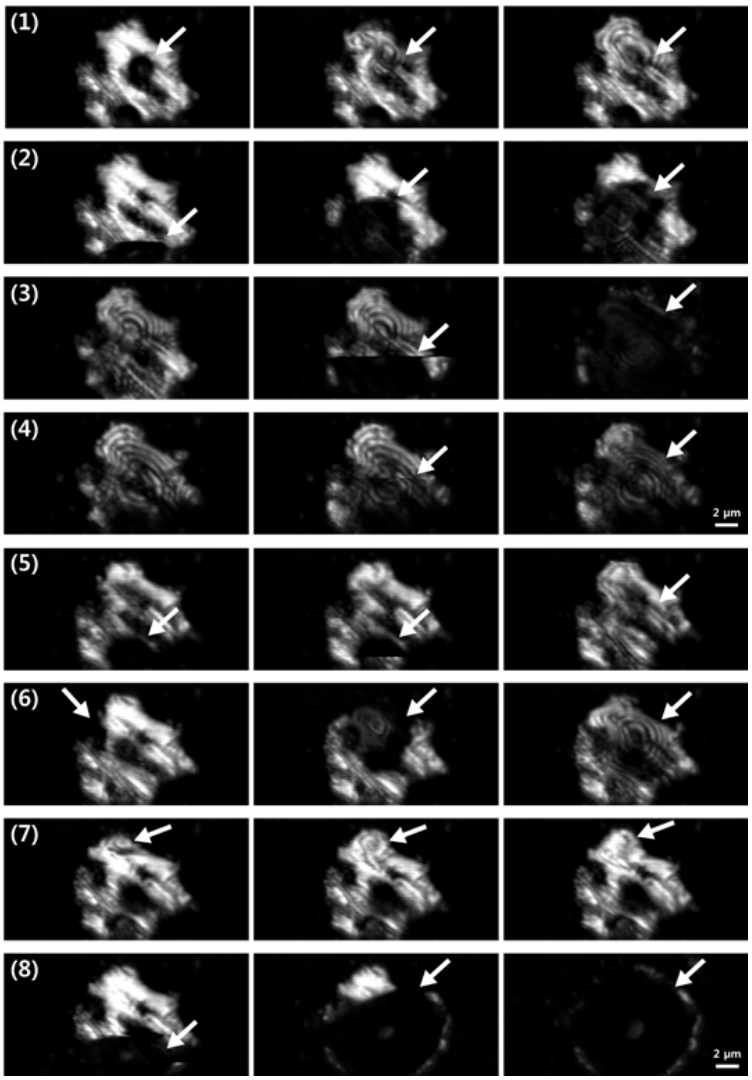

Fig. 3-23 Sequence of images at the number shown in Fig. 3-22. A droplet collides with surface of a Pt UME. White arrows indicate the position of the targeted droplet. A 1.0 V was applied to the electrode, and each sequence of images were collected at intervals of 0.0195 s, Scale bar = 2 μm

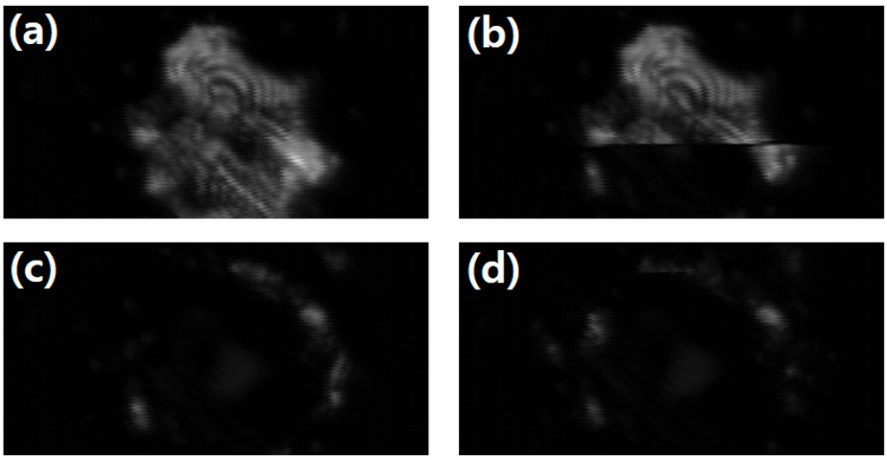

Fig. 3-24 The confocal microscopy images of the spike at 22.24 s, which is the largest spike in Fig. 3-21. Images of just before the emulsion collision (a) 22.20 s, (b) 22.22s. An image at collision moment (c) 22.24s. The image for the next spike in the i-t curve (d) 22.76 s.

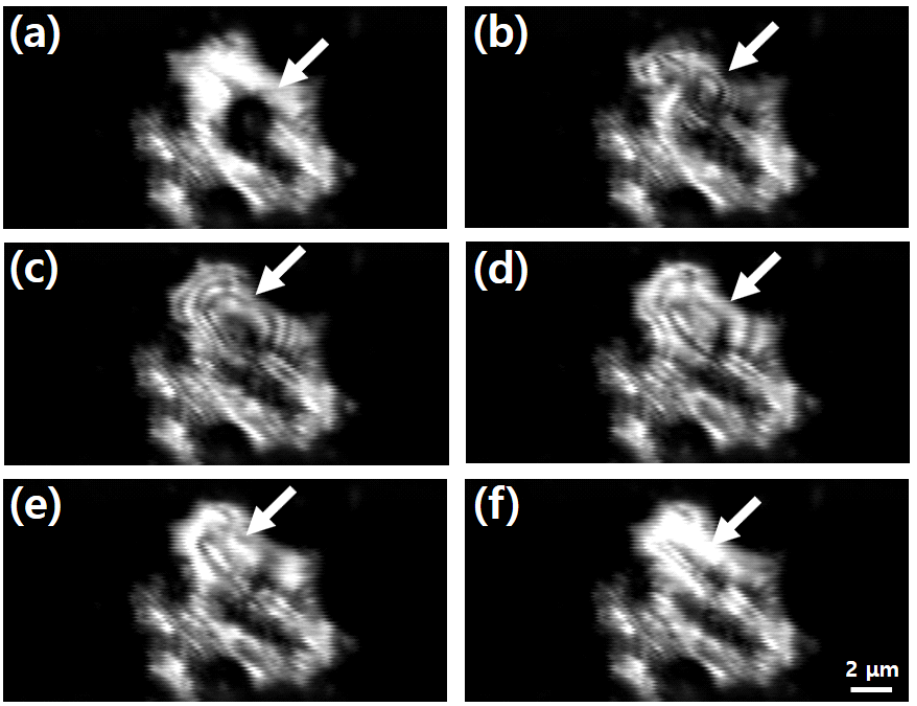

Fig. 3-25 Images of the moment a droplet collides with the surface of a Pt UME. White arrows indicate the position of the droplet traced. The time elapsed at 1.0 V is (a) 20.19 s, (b) 20.21 s, (c) 20.23 s, (d) 20.31 s, (e) 20.36 s, (f) 20.42 s, respectively. Scale bar = 2 μm

Fig. 3-25 show how a droplet collides with the UME. The collision of droplet occurs at 20.21 s and corresponds to the red dot mark at the same time in Fig. 3-21. This agrees with the result observed at the Pt wire electrode shown in Fig. 3-16. Figures Fig. 3-25a and 3-25b show a droplet approaching and colliding with the electrode surface, respectively. The droplet spreads out and sticks to the electrode surface and gradually fade away (Fig. 3-25c, d, e and f). There are other examples of droplet collision with the Pt UME in Fig. 3-26 to 3-28.

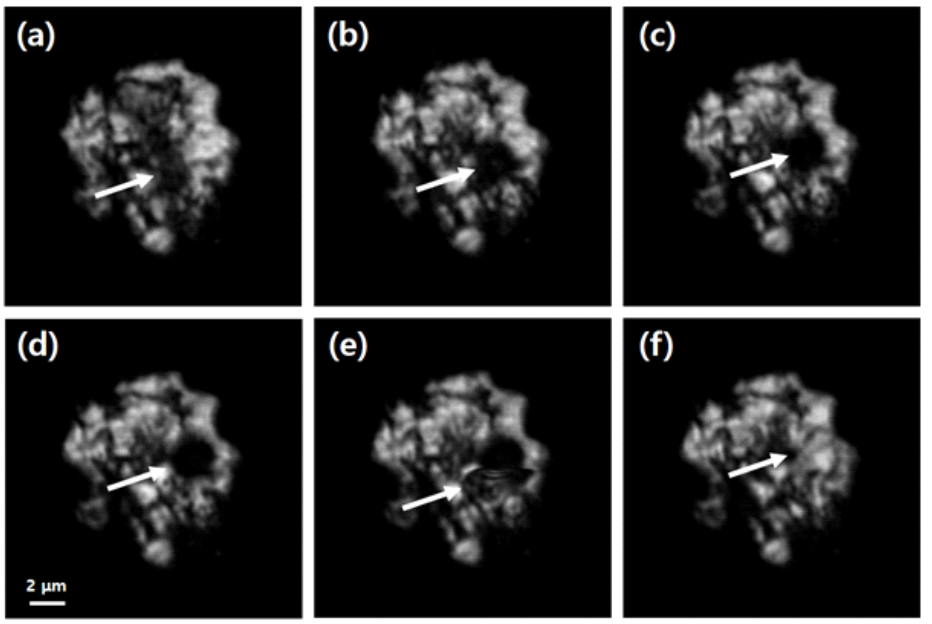

Fig. 3-26 Images at the moment the emulsion collides with the surface of a Pt UME. White arrows indicate the position of the targeted droplet. A 1.0 V was applied to the electrode. The entire images, out of which 6 images were selected, were collected at intervals of 0.15 s. The time from the first image is (a) 0 s, (b) 1.48 s, (c) 2.74 s, (d) 3.48 s, (e) 3.58 s, (f) 3.69 s, respectively. Scale bar = 2 μ m.

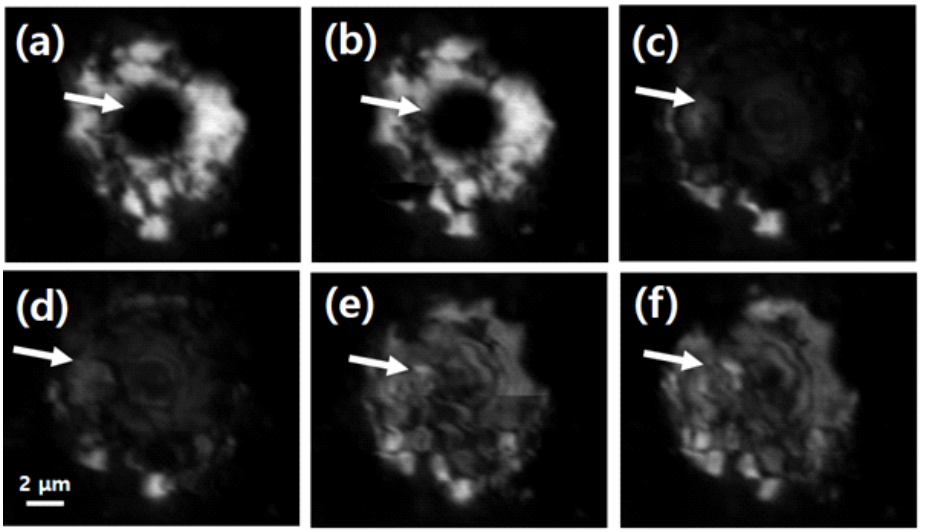

Fig. 3-27 Images at the moment the emulsion collides with the surface of a Pt UME. White arrows indicate the position of the targeted droplet. A 1.0 V was applied to the electrode. The entire images, out of which 6 images were selected, were collected at intervals of 0.15 s. The time from the first image is (a) 0 s, (b) 0.3 s, (c) 0.45 s, (d) 1.2 s, (e) 1.95 s, (f) 2.85 s, respectively. Scale bar = 2 μ m.

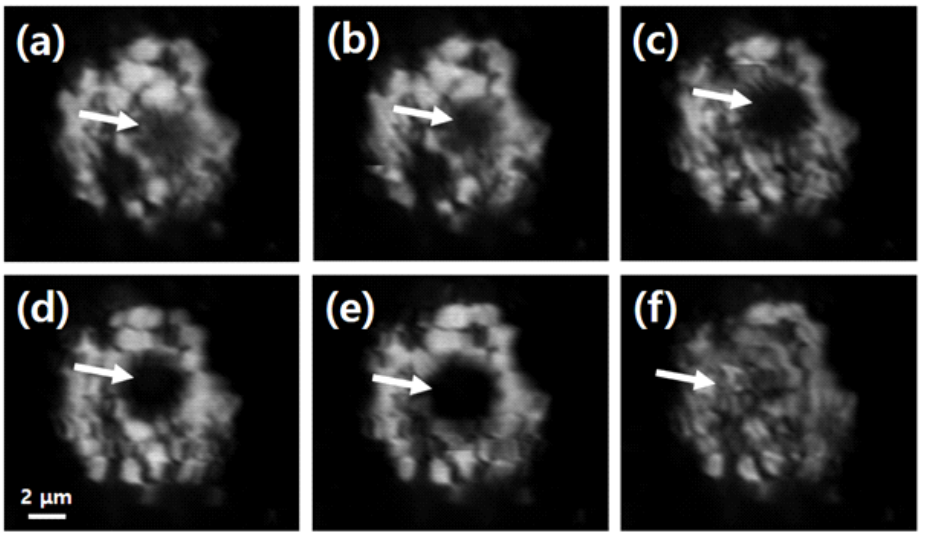

Fig. 3-28 Images at the moment the emulsion collides with the surface of a Pt UME. White arrows indicate the position of the targeted droplet. A 1.0 V was applied to the electrode. The entire images, out of which 6 images were selected, were collected at intervals of 0.15 s. The time from the first image is (a) 0 s, (b) 0.60 s, (c) 1.35 s, (d) 1.65 s, (e) 2.84 s, (f) 2.99 s, respectively. Scale bar = 2 μ m.

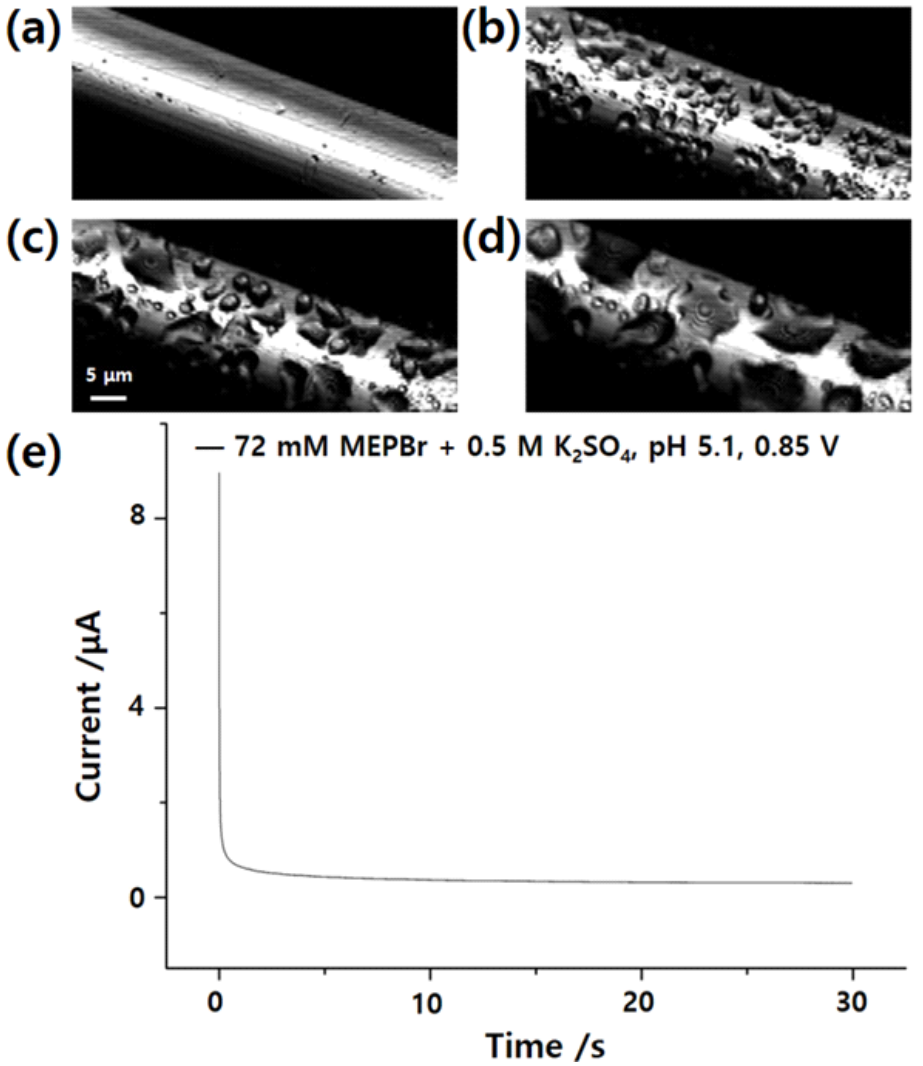

Fig. 3-29 Chronoamperogram and confocal microscopy images at the moment the droplets grow on the surface of a Pt wire electrode. The time elapsed at 0.85 V (a) 0 s, (b) 5 s, (c) 15 s, (d) 30 s, respectively. Scale bar = 5 μm. (e) Chronoamperogram at 0.85 V

From 0.85 V to 0.9 V, where the current starts to increase on cyclic voltammogram (**Fig. 3-7 and 3-8**), the droplets tend to grow at the electrode. (**Fig. 3-29**) In this potential range, the current is larger than that of KBr solution. At 1.0 V, the droplet collides with the electrode and generates a current spike. There are some explanations about the current increase phenomenon caused by droplets. The first is that Br^- diffuses from the aqueous solution and is concentrated in the droplet. This is supported by the studies on current spikes using bulk electrolysis model and simulation, although they provide indirect evidences. [29, 37] In **Fig. 3-21** and **3-25**, it is apparent that spike current appears when the droplets collide with electrode, implying that higher concentration of Br^- makes current increase. Another possibility is the acceleration of transport process by the rapid exchange reaction of the Br^--Br_3^- couple. The diffusion of Br^- can be accelerated by Br_3^- owing to the equilibrium $Br_3^- \leftrightharpoons Br_2 + Br^-$. [38, 39] Since the MEP$Br_3$ droplet has a large number of Br_3^-, it is highly probable that the diffusion of Br^- in the droplet is accelerated and thereby

current increases. The third is the effect of enlarged electrode area by the droplets. We can imagine that the effective electrode area increases when the droplet grows or collides on the electrode surface, which is reminiscent of insoluble redox film on the electrode or Hg deposited on the UME. [40-43] This scenario is less probable, however, as indicated by the observation that the size of the droplet and the area covering the electrode increase at 0.85 V, while the current decreases. (**Fig. 3-29**) Overall, this issue is still open, requiring further study.

Consequently, *in-situ* confocal microscopy allows us to see how emulsion droplet behaves near the electrode surface with several μm and tens of ms of spatial and temporal resolutions, respectively, which are sufficient for investigating Br^- electrochemistry.

3.4 Conclusion

We introduced confocal microscopy to investigate formation, diffusion, and collision of $MEPBr_3$ droplets in the electrochemical system. Confocal images and voltammograms from a wire and a UME of Pt unambiguously told that the droplets are generated heterogeneously on the electrode surface and adsorbed onto the electrode. Emulsion appears at 0.925 V or higher and some of the resulting droplets collide with the electrode surface. The confocal images and chronoamperogram, simultaneously acquired from the Pt UME, ensure that collisions of droplets produce the spikes. Oxidative current increases whenever $MEPBr_3$ droplet touches the electrode surface regardless of adsorption or collision. Colliding with the electrode surface leads to current surge up to 7.38 times from the baseline of the chronoamperogram. These results are compelling evidences supporting that electrochemistry at the interface between the electrode and the droplet makes significant contribution to overall Br^- oxidation reaction. This may suggest paths to

better bromine–complex agents for the redox flow batteries. Although what causes the current augmentation is still unanswered requiring further study, in particular electrokinetic investigation, the observations in this work are expected to be a cornerstone to achieve deeper understanding of the Br^- oxidation in the $MEPBr_3$ droplet, eventually resulting in advance of the redox flow batteries.

3.5 References

[1] Rees, N. V., *Electrochem. Commun.,* 2014, *43*, 83.

[2] Cheng, W., Compton, R. G., *TrAC, Trends Anal. Chem.,* 2014, *58*, 79.

[3] Zhou, Y.-G., Rees, N. V., Compton, R. G., *Angew. Chem. Int. Ed.,* 2011, *50*, 4219.

[4] Stuart, E. J. E., Zhou, Y.-G., Rees, N. V., Compton, R. G., *RSC Advances,* 2012, *2*, 6879.

[5] Ellison, J., Tschulik, K., Stuart, E. J. E., Jurkschat, K., Omanović, D., Uhlemann, M., Crossley, A., Compton, R. G., *ChemistryOpen,* 2013, *2*, 69.

[6] Kwon, S. J., Fan, F.-R. F., Bard, A. J., *J. Am. Chem. Soc.,* 2010, *132*, 13165.

[7] Xiao, X., Bard, A. J., *J. Am. Chem. Soc.,* 2007, *129*, 9610.

[8] Xiao, X., Fan, F.-R. F., Zhou, J., Bard, A. J., *J. Am. Chem. Soc.,* 2008, *130*, 16669.

[9] Hellberg, D., Scholz, F., Schauer, F., Weitschies, W., *Electrochem. Commun.,* 2002, *4*, 305.

[10] Cheng, W., Compton, R. G., *Angew. Chem. Int. Ed.,*

2014, *53*, 13928.

[11] Dunevall, J., Fathali, H., Najafinobar, N., Lovric, J., Wigström, J., Cans, A.-S., Ewing, A. G., *J. Am. Chem. Soc.,* 2015, *137*, 4344.

[12] Oleinick, A., Lemaitre, F., Collignon, M. G., Svir, I., Amatore, C., *Faraday Discuss.,* 2013, *164*, 33.

[13] Dick, J. E., Hilterbrand, A. T., Boika, A., Upton, J. W., Bard, A. J., *Proc. Natl. Acad. Sci. U. S. A.,* 2015, *112*, 5303.

[14] Dick, J. E., Renault, C., Bard, A. J., *J. Am. Chem. Soc.,* 2015, *137*, 8376.

[15] Kim, B.-K., Boika, A., Kim, J., Dick, J. E., Bard, A. J., *J. Am. Chem. Soc.,* 2014, *136*, 4849.

[16] Kim, B.-K., Kim, J., Bard, A. J., *J. Am. Chem. Soc.,* 2015, *137*, 2343.

[17] Li, Y., Deng, H., Dick, J. E., Bard, A. J., *Anal. Chem.,* 2015, *87*, 11013.

[18] Yang, Z., Zhang, J., Kintner-Meyer, M. C. W., Lu, X., Choi, D., Lemmon, J. P., Liu, J., *Chem. Rev.,* 2011, *111*, 3577.

[19] Skyllas-Kazacos, M., Chakrabarti, M. H., Hajimolana, S.

A., Mjalli, F. S., Saleem, M., *J. Electrochem. Soc.,* 2011, *158*, R55.

[20] Weber, A. Z., Mench, M. M., Meyers, J. P., Ross, P. N., Gostick, J. T., Liu, Q., *J. Appl. Electrochem.,* 2011, *41*, 1137.

[21] Alotto, P., Guarnieri, M., Moro, F., *Renew. Sust. Energ. Rev.,* 2014, *29*, 325.

[22] Eustace, D. J., *J. Electrochem. Soc.,* 1980, *127*, 528.

[23] Mastragostino, M., Valcher, S., *Electrochim. Acta,* 1983, *28*, 501.

[24] Skyllas-Kazacos, M., Kazacos, G., Poon, G., Verseema, H., *Int. J. Energ. Res.,* 2010, *34*, 182.

[25] Kalu, E. E., White, R. E., *AlChE J.,* 1991, *37*, 1164.

[26] Kautek, W., Conradi, A., Sahre, M., Fabjan, C., Drobits, J., Bauer, G., Schuster, P., *J. Electrochem. Soc.,* 1999, *146*, 3211.

[27] Kautek, W., Conradi, A., Fabjan, C., Bauer, G., *Electrochim. Acta,* 2001, *47*, 815.

[28] Lancry, E., Magnes, B.-Z., Ben-David, I., Freiberg, M., *ECS Transactions,* 2013, *53*, 107.

[29] Park, S., Kim, H., Chae, J., Chang, J., *J. Phys. Chem. C,*

2016, *120*, 3922.

[30] Dick, J. E., Renault, C., Kim, B.-K., Bard, A. J., *Angew. Chem. Int. Ed.,* 2014, *53*, 11859.

[31] Fosdick, S. E., Anderson, M. J., Nettleton, E. G., Crooks, R. M., *J. Am. Chem. Soc.,* 2013, *135*, 5994.

[32] Shan, X., Patel, U., Wang, S., Iglesias, R., Tao, N., *Science,* 2010, *327*, 1363.

[33] Shan, X., Diez-Perez, I., Wang, L., Wiktor, P., Gu, Y., Zhang, L., Wang, W., Lu, J., Wang, S., Gong, Q., Li, J., Tao, N., *Nat. Nano,* 2012, *7*, 668.

[34] Fang, Y., Wang, W., Wo, X., Luo, Y., Yin, S., Wang, Y., Shan, X., Tao, N., *J. Am. Chem. Soc.,* 2014, *136*, 12584.

[35] Hill, C. M., Pan, S., *J. Am. Chem. Soc.,* 2013, *135*, 17250.

[36] Wang, Y., Shan, X., Cui, F., Li, J., Wang, S., Tao, N., *Anal. Chem.,* 2015, *87*, 494.

[37] Park, S., Shin, S., Jung, D., Chae, J., Chang, J., *J. Electroanal. Chem.*, 2017, *797*, 97.

[38] Ruff, I., Friedrich, V. J., Csillag, K., *J. Phys. Chem.*,

1972, *76*, 162.

[39] Ruff, I., Friedrich, V. J., *J. Phys. Chem.*, 1972, *76*, 2957.

[40] Scharifker, B., Wehrmann, C., *J. Electroanal. Chem.*, 1985, *185*, 93.

[41] Lee, C., Lee, Y. K., Lee, Y., Jeon, I. C., *J. Electroanal. Chem.*, 1999, *463*, 224.

[42] Mauzeroll, J., Hueske, E. A., Bard, A. J., *Anal. Chem.*, 2003, *75*, 3880.

[43] Scharifker, B., Hills, G., *J. Electroanal. Chem.*, 1981, *130*, 81.

4. Summary and Perspectives

This dissertation discusses the electrochemical properties of nanoparticles and microemulsions. Nanoparticles and microemulsions are used as the catalysts or additives in the field of energy conversion and storage devices; they promote electrochemical reactions or participate in reactions with special purpose such as capturing by-product. However, most studies on energy conversion focused on the development of new materials. As a result, the mechanism of electrochemical reactions involving small particles is still veiled. Therefore, we tried to establish a new breakthrough by studying the underlying mechanisms of small particles causing or participating in electrochemical reactions.

In Chapter 2, we investigated the electrochemical characteristics of Au NPs, which are known to have a better catalytic activity than bulk materials. The prepared Au NPs had finely tuned diameter and interparticle spacing without aggregation. The electrochemical oxidation characteristics of the synthesized Au NP arrays were analyzed by stripping

voltammetry. The results confirmed that the coverage, total amount of gold on the substrate, is a more influential factor for the electrooxidation reaction of Au NPs when the particle size and spacing are controlled.

In Chapter 3, electrogenerated microemulsion, $MEPBr_3$, was simultaneously investigated by confocal microscopy and chronoamperometry. In this way, we confirmed the formation, diffusion and collision of the emulsion with the electrode surface. Confocal images and voltammograms from a wire and a ultramicroelectrode of Pt unambiguously show that the emulsions are generated heterogeneously on the electrode surface and adsorbed onto the electrode. Emulsions appear at the critical potential (0.925 V vs Ag/AgCl) or higher and some of the desorbed emulsions collide with the electrode surface. The confocal images and chronoamperogram, simultaneously acquired from the Pt ultramicroelectrode, show that a collision of emulsion produces a current spike. The oxidation current increased when the emulsion was adsorbed on or collided with the electrode and increased up to 7.38 times the baseline of

chronoamperogram when the emulsion collided with the electrode. These results show significant contribution of $MEPBr_3$ emulsion to overall Br^- oxidation reaction and electrochemical feature of $MEPBr_3$ emulsions.

From the aforementioned researches, it is possible to apply the result of the fundamental study on the oxidation of Au NPs to design a catalyst to prevent the oxidation of NPs, which may be a problem when the metal NPs are used as the catalyst. Also, the study on the electrochemical contribution of $MEPBr_3$ emulsion electrochemically generated by adding it as an additive to redox flow batteries can be applied to design a material that can function not only as an additive but also as a catalyst for the efficient Br^-/Br_2 electrochemical reaction.

국문초록

화석 연료의 고갈과 환경 오염으로 인한 문제를 해결하기 위해 지난 수십년간 화석 연료를 대체하기 위한 에너지에 대한 연구는 가장 중요한 연구 주제 중 하나였다. 그런 노력에도 불구하고, 여전히 대부분의 에너지는 화석연료로 소비되고 있으며 에너지 소비도 전 세계적으로 꾸준히 증가하고 있는 추세이다. 따라서 새로운 에너지 변환 및 저장 장치에 대한 연구는 더욱 중요해 질 것이다.

에너지 변환 장치에서 중요한 요소 중 하나는 전기화학 반응이 일어나는 촉매 물질이다. 이런 촉매 물질의 효율을 향상시키기 위한 방법으로 나노 입자 (nanoparticle) 를 합성하여 응용하는 연구가 최근 많이 발표되고 있다. 이런 나노 입자는 벌크 물질과는 다른 물리적, 화학적 성질을 가진 것으로 알려져 왔고, 부피에 비하여 표면적이 매우 넓은 구조를 가지고 있고 표면에 지배적인 특성 때문에 전기화학적 활성도 뛰어나다. 그러나 이런 나노 입자가 전기화학 환경에 있을 때 어떤 특성을 가지며 그런 특성의 원인은 무엇인가에 대한 이해는 아직 완전히 이루어지지 못하였다.

또 다른 관점에서 에너지 저장 장치도 주목을 받고 있다. 일반적으로 에너지는 전기의 형태로 소비되며 전기 에너지의 공급과 소비는 항상 균형을 이루지 못한다. 이런 문제를 효과적으로 해결하기

위해서 남는 전기를 저장해두었다가 필요할 때 꺼내 쓰는 전기 에너지 저장 시스템의 필요성이 대두되고 있다. 다양한 에너지 저장 기술들 중 redox flow battery는 저장하는 에너지의 전력과 전력량을 용이하게 조절할 수 있는 장점 때문에 각광받고 있다. 대표적인 redox flow battery로 Br−polysurfide, Zn−Br 등이 있는데 이런 시스템들은 Br^-/Br_2 의 산화, 환원 반응을 이용하는 것이다. 이 시스템들의 문제점중 하나는 전기화학적으로 생성된 Br_2 가 분리막을 통과하여 자가 방전을 일으키는 것이다. 이를 방지하기 위해 Br_2를 붙잡아 마이크로 에멀션 (microemulsion) 을 형성하는 quaternary ammonium bromides를 첨가해준다. 그런데 최근 이 에멀션이 단순히 Br_2를 붙잡는 역할뿐만 아니라 전기화학 반응에 참여한다는 것이 보고되었으나 그 매커니즘은 확실하지 않다.

이처럼 에너지 변환 및 저장 장치에 나노 입자와 마이크로 에멀션과 같은 작은 크기의 입자들이 전기화학 반응에 참여하여 기여하고 있으나 많은 연구들은 재료적인 측면에 초점이 맞춰져 있고 작은 입자들의 역할과 전기화학적 특성에 대한 근본적인 이해는 부족하다. 본 학위 논문은 에너지 변환 및 저장 장치와 관련된 작은 입자들의 전기화학적 특성에 관한 두 가지 연구 사례를 포함하고 있다.

첫째, 전기화학 환경에서 금 나노 입자의 산화 안정성에 관해 연

구하였다. 이중블록공중합체를 이용하여 크기와 입자간 간격을 나노미터 수준으로 균일하게 조절할 수 있는 나노 입자의 집합체를 평면 전극위에 합성하고 이를 이용하여 입자의 크기와 간격에 따른 산화 반응성의 변화를 관찰하였다. Surface coverage는 기저 전극위에 합성된 금의 총량을 표현하는 말로 입자의 크기와 간격을 조절함에 따라 함께 변하는 변수이다. 순수하게 금 표면이 드러난 나노 입자들의 전기화학 산화 특성을 살펴보았을 때 실험 조건에서 입자의 크기보다 금의 총량인 surface coverage가 산화 반응에 영향을 끼치는 주된 원인임을 확인하였다.

둘째, redox flow battery에서 사용되는 bromine complex agent가 어떻게 전기화학적으로 에멀션을 형성하고 어떻게 그 에멀션이 Br^-/Br_2 반응에 참여하는지를 연구하였다. 에멀션의 전기화학적 특성을 연구하기 위하여 시간전류법 (chronoamperometry) 과 공초점 현미경 (confocal microscopy) 을 동시에 측정하였다. 이 실험결과들로 에멀션이 전극 표면에서 생성되며 생성된 에멀션이 전극위에 흡착되어 있을 때도 산화 전류가 증가한다는 사실을 확인하였다. 그리고 시간전류법을 이용하여 전류를 측정하였을 때 발생하는 급격한 전류 증가가 에멀션의 충돌에 의한 것임을 공초점 현미경으로 확인하였다. 이를 통해 에멀션의 생성과 충돌이 Br^- 산화 반응에 큰 영향을 끼침을 증명하였다.

이러한 연구는 보다 근원적이고 기초적인 연구를 통해 널리 응용되고 있는 작은 입자들이 작용하는 기저 매커니즘을 이해함으로써 에너지 변환 및 저장 장치의 연구 및 개발에 새로운 방향을 제시할 수 있음을 보여줄 것이라 기대된다.

주요여: 에너지 변환 및 저장 장치, 촉매, 나노 입자, 마이크로 에멀션, 공초점 현미경, 전기화학 특성

학번: 2011-20312